Corrosion Mechanisms in Zirconium Alloys

Authors

Ron Adamson
Zircology Plus, Fremont, CA, USA

Friedrich Garzarolli
Erlangen, Germany

Brian Cox
University of Toronto, ON, Canada

Alfred Strasser
Aquarius Services, Sleepy Hollow, NY, USA

Peter Rudling
ANT International, Skultuna, Sweden

Reviewed by

Ron Adamson
Zircology Plus, Fremont, CA, USA

A.N.T. INTERNATIONAL®

● October 2007
Advanced Nuclear Technology International
Krongjutarvägen 2C, SE-730 50 Skultuna
Sweden

info@antinternational.com
www.antinternational.com

Disclaimer

The information presented in this report has been compiled and analysed by Advanced Nuclear Technology International Europe AB (*ANT* International) and its subcontractors. *ANT* International has exercised due diligence in this work, but does not warrant the accuracy or completeness of the information. *ANT* International does not assume any responsibility for any consequences as a result of the use of the information for any party, except a warranty for reasonable technical skill, which is limited to the amount paid for this assignment by each *ZIRAT* programme member.

Acronyms and Explanations

ANT	Advanced Nuclear Technology
AOA	Axial Offset Anomaly
ASTM	American Society for Testing and Materials
ATR	Advanced Test Reactor
BOC	Beginning of Cycle
BWR	Boiling Water Reactor
CANDU	Canadian Deuterium Uranium
CILC	Crud Induced Localized Corrosion
CRUD	Chalk River Unidentified Deposits
DCP	Distinctive Crud Pattern
DX	Duplex
ECCS	Emergency Core Cooling System
ELS	Extra-Low Sn
EOC	End Of Cycle
ESSC	Enhanced Spacer Shadow Corrosion
FDI	Fuel Duty Index
GB	Grain Boundaries
GE	General Electric
GNF	Global Nuclear Fuel
HBWR	Halden BWR
HF	High Frequency
HPA	High Performance Alloy
HPUF	Hydrogen PickUp Fraction
HWC	Hydrogen Water Chemistry
IAEA	International Atomic Energy Agency
KKL	KernKraftwerk Leibstadt
LHGR	Linear Heat Generation Rate
LK	Låg corrosion (Low Corrosion in Swedish)
LL	Low Leakage
LWR	Light Water Reactor
NMCA	Noble Metal Chemical Addition
NSSS	Nuclear Steam Supply System
NWC	Normal Water Chemistry
OI	Out-In
PIE	Post-Irradiation Examinations
PT	Pressure Tube
PWR	Pressurised Water Reactor
RBMK	Reaktor Bolshoi Mozhnosti Kanalov (in English Large Boiling Water Channel type reactor)
RT	Room Temperature
RXA	Recrystallised Annealed
SEM	Scanning Electron Microscopy
SGHWR	Steam Generating Heavy Water Reactor
SHE	Standard Hydrogen Electrode
SIMS	Secondary Ion Mass Spectroscopy
SPP	Second Phase Particle
SRA	Stress Relieved Annealed
SS	Stainless Steel
STEM	Scanning Transmission Electron Microscopy
STR	Special Topic Report
TEM	Transmission Electron Microscopy
TM	Transition Metal
TMI	Three Mile Island

TSS	Terminal Solid Solubility
TZP	Tetragonal Zirconia Polycrystal
VVER	Voda Voda Energo Reactor (Russian type *PWR*)
YSZ	Yttria Stabilised Zirconia
ZIRAT	Zirconium Alloy Technology
ZIRLO	Zirconium Low Oxidation

Unit Conversion

TEMPERATURE

°C + 273.15 = K

°C*1.8 +32 = °F

T(K)	T(°C)	T(°F)
273	**0**	32
289	16	61
298	25	77
373	**100**	212
473	**200**	392
573	**300**	572
633	360	680
673	**400**	752
773	**500**	932
783	510	950
793	520	968
823	550	1022
833	560	1040
873	**600**	1112
878	605	1121
893	620	1148
923	650	1202
973	**700**	1292
1023	750	1382
1053	780	1436
1073	**800**	1472
1136	863	1585
1143	870	1598
1173	**900**	1652
1273	**1000**	1832
1343	1070	1958
1478	1204	**2200**

DISTANCE

x (µm)	x (mils)
0.6	0.02
1	0.04
5	0.20
10	0.39
20	0.79
25	0.98
25.4	**1.00**
100	3.94

PRESSURE

bar	MPa	psi
1	0.1	14
10	**1**	142
70	7	995
70.4	7.04	**1000**
100	10	1421
130	13	1847
155	15.5	2203
704	70.4	**10000**
1000	100	14211

MASS

kg	lbs
0.454	**1**
1	2.20

STRESS INTENSITY FACTOR

MPa√m	ksi√inch
0.91	**1**
1	1.10

Radioactivity

1 Sv = 100 Rem

1 Ci = 3.7 x 1010 Bq = 37 GBq

1 Bq = 1 s^{-1}

Contents

1 Introduction (Ron Adamson)

The emphasis of this Special Topical Report (*STR*) is on the *mechanisms* of corrosion of zirconium alloys used in the core of nuclear power plants. The entire area of corrosion (and the accompanying absorption of hydrogen in the zirconium metal matrix) is of prime interest when considering performance of the core components and therefore the performance of the entire reactor. For instance, for Pressurised Water Reactors (*PWR*s) a practical corrosion limit exists (about 100 μm oxide thickness which is associated with a critical amount of hydrogen absorption) that has driven a material change away from Zircaloy-4.

The technical literature and many conferences are full of papers dealing with corrosion issues. of particular interest is the series "Zirconium in the Nuclear Industry: International Symposium", *ASTM* STP, American Society of Testing and Materials, which provides most relevant details. Also reviews of the topic are given in Adamson et al., 2002 ("Corrosion of Zirconium Alloys", Zirconium Alloy Technology (*ZIRAT7*) Special Topics Report, December, 2002) and "Waterside corrosion of zirconium alloys in nuclear power plants", International Atomic Energy Agency (*IAEA*)-TECDOC-996, January 1998. The current *STR* deals only lightly with general corrosion phenomena, with the aim being to concentrate on corrosion mechanisms. The most recent open literature review of mechanisms is Cox, 2005.

Corrosion of zirconium alloys is an electrochemically-driven process affected by the microstructure and microchemistry of the alloy surface, the nature of the oxide layer that forms, the temperature at the metal/oxide interface, the chemistry and thermohydraulics of the corrodent water, the effects of irradiation and the effects of time.Specifics of these processes are given later in this STP; some general introduction is given here.

Table 1-1 gives information on the various types of commercial power reactor systems currently being used throughout the world. In comparing Boiling Water Reactor (*BWR*s) with *PWR*s, with corrosion mechanisms in mind, the main features are:

- *BWR* coolant boils; *PWR* coolant does not. This has an important effect at the oxide/water interface.
- *PWR* coolant contains a high concentration of hydrogen; *BWR* coolant does not. Complementarily, *BWR* coolant contains a high concentration of oxygen, *PWR* coolant does not. This has an important effect on corrosion processes.
- *PWR* components generally operate at higher temperatures than *BWR* components. Corrosion processes are temperature dependent.
- Both reactor types employ chemical additions to the coolant which may effect corrosion and build-up of deposits on fuel rods.

Table 1-1: Design Parameters for water cooled reactors, Adamson et al., 2002.

Parameter	Western type *PWR*	*VVER* (440/1000) MW	CANDU[1]	*BWR*	*RBMK*[2]
1. Coolant	Pressurized H_2O	Pressurized H_2O	Pressurized D_2O	Boiling H_2O	Boiling H_2O
2. Fuel Materials (Pressure tube materials)	Zry-4, *ZIRLO*, DUPLEX, M5, Inconel, *SS*[3]	Zr-alloy E110	Zry-4 (Zr2.5Nb)	Zry-2, Zry-4, Inconel, *SS*	Zr-alloy E110, (Zr2.5Nb)
3. Average power rating, (kW/l)	80-125	83/108	9-19	40-57	5
4. Fast Neutron Flux, Average, n/cm².s	6-9E13	5E13/7E13	1.5-2E12	4-7E13	1-2E13
5. Temperatures, °C					
Average Coolant inlet	279-294	267/290	249-257	272-278	270
Average Coolant outlet	313-329	298/320	293-305	280-300	284
Max Cladding OD	320-350	335/352	310	285-305	290
Steam mass content, %				7-14	14
6. System pressure, bar	155-158	125/165	96	70	67
7. Coolant Flow, m/s	3-6*	3.5/6	3-5	2-5*	3.7
8. Coolant Chemistry**					
Oxygen, ppb	<0.05	<0.1		200-400	<20
Hydrogen (D_2), ppm	2-4		(3-10)	.05-.30	-
cc/kg	25-50	30-60			
Boron (as Boric acid), ppm	0-2200	0-1400	-	-	-
Li (as LiOH), ppm	0.5-3.5	0.05-0.6	1	-	-
K (as KOH), ppm	-	5-20		-	-
NH_3, ppm		6-30			
NaOH, ppm		0.03-0.35			

[1]Canadian Deuterium Uranium (CANDU), [2]Reaktor Bolshoi Mozhnosti Kanalov (RBMK), [3]Stainless Steel (SS), [4]Voda Voda Energo Reactor (VVER), [5]Zirconium Low Oxidation (*ZIRLO*)

It also should be noted that *BWR* zirconium alloys continue to be primarily Zircaloy-2 or slight variants of Zircaloy-2. *PWR* zirconium alloys no longer tend to be Zircaloy-4, for reasons of insufficient corrosion resistance (and hydriding resistance) at high burn-up, but have moved toward zirconium alloys with Nb additions.

---

* Variation from lower to upper part of the core and from plant to plant.
* Variation from lower to upper part of the core and from plant to plant.
** Zn in ppb quantities may be added for *BWR*s and *PWR*s; Pt and Rh in ppb quantities may be added for *BWR*s.

The type of oxides which form during corrosion in reactor water can be classified into several categories. The two most basic are uniform and nodular corrosion. The "uniform" category has an extension – "patch" or accelerated uniform. The fourth category is "shadow corrosion", which can look like thick uniform corrosion but has some characteristics of nodular corrosion. The fifth category is crud- related corrosion, which is a temperature driven process induced by poor heat transfer in crud-impregnated corrosion layers. These categories will be discussed later, but will be introduced here. Table 1-2 (Garzarolli in Adamson et al., 2002) gives a useful summary of characteristics of various corrosion types.

Table 1-2: Types of corrosion observed for Zircaloy in-reactor and out-of-reactor, Garzarolli in *ZIRAT7 STR* "Corrosion in Zirconium Alloys", Adamson et al., 2002.

Type of corrosion	Comment	Observed	Irradiation effect in oxygenated coolant (*BWR*)	Irradiation effect in hydrogenated coolant *PWR*
Uniform	Normal mode	Out-of-pile, in-*BWR* and, in-*PWR*	5-10x increased from beginning, low flux dependency	2-4x increased after 1st corrosion rate transition, low flux dependency
Nodular	Local break down of oxide protectivness	In-*BWR* and out-of-pile >500°C, Zry with large *SPP*	Increases almost linear with fast flux, little temp. dependency	not observed
Shadow corrosion	Probably driven by potential differences	Only under irradiation and oxidative coolant conditions (*BWR*)	Increases probably almost linear with fast flux	not observed
Crevice corrosion	Change of environment in small gaps	Out-of-pile, in-*BWR* and, in-*PWR*	observed	Observed
Increased corrosion with fine *SPP*	Reduction of protectivity	Out-of-pile, in-*BWR* and, in-*PWR*	Increases almost linear with fast flux	Increases almost linear with fast flux, little temp. dependency
Increased corrosion at high fluences	Reduction of protectivity	In-*PWR*	?	Increases with increasing fluence above a critical threshold
Increased corrosion at high hydride concentrations	Lower corrosion resistance of hydride	Out-of-pile, in-*BWR* and, in-*PWR*	observed	Flux dependent but less temperature dependent

Uniform corrosion occurs in both *PWR*s and *BWR*s. The oxide itself is uniform in thickness and consists of several different layers, discussed in Section 2. For either in or out of reactor, the initial shape of the corrosion-versus-time curve is as shown in Figure 1-1 in the pre-transition region. The transition point occurs at around 5 µm oxide thickness in *PWR*s. The shape of the post-transition curve in *PWR*s depends on several variables: initial Second Phase Particle (*SPP*) size, irradiation, amount of cold work, specific alloy, water chemistry, temperature, local thermohydraulics, hydride concentration – all to be discussed in Section 3. For Zircaloy-4 the corrosion thickness at high burn-up may reach or exceed 100 µm, while some of the newer alloys have less than half of that. As noted in Table 1-2, only uniform corrosion occurs in *PWR*s under non-boiling, hydrogenated conditions.

The study of uniform corrosion in the laboratory at temperatures relevant to reactor operation suffers from three problems: 1) irradiation effects are absent, 2) corrosion rates are very low at 280°C (553K) - 360°C (633K), 3) very long times (hundreds of days) are required to differentiate between material variables. The most widely used test appears to be 360°C (633K) pressurized water for very long times. An example is given in Figure 1-2, where a series of Zircaloy-type alloys with different Sn contents are compared. Garde et al., 1994, show that in-reactor results after high burn-up give the same ranking as the autoclave laboratory tests. Also for *PWR*s, adding Li to the water is thought to improve comparisons, Sabol et al., 1994.

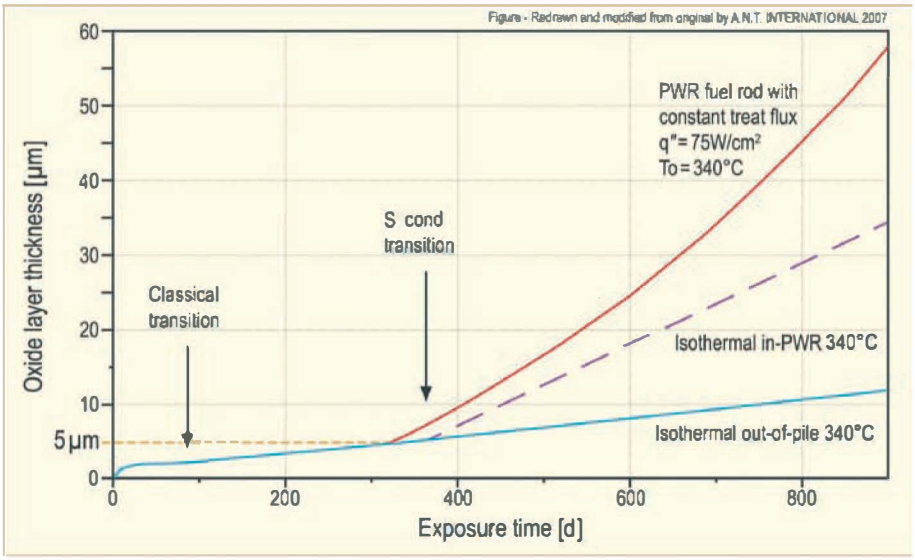

Figure 1-1: Schematic of *PWR* corrosion kinetics, Garzarolli et al., 1996.

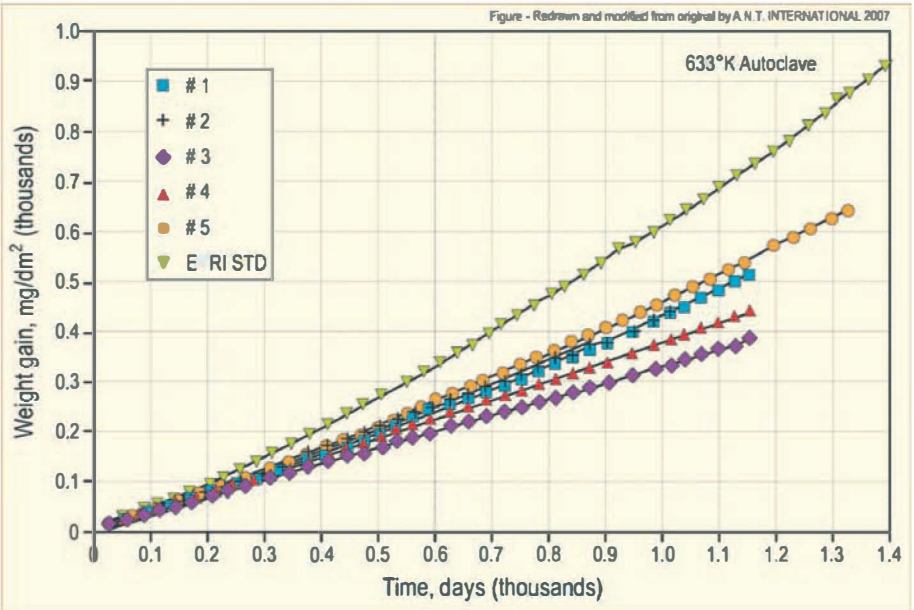

Figure 1-2: Corrosion weight gain as a function of laboratory autoclave test exposure time for several Zircaloy-4 tube variants, Garde et al., 1994.

Both Zircaloy-2 and -4 form a protective uniform oxide in typical *BWR*s and *PWR*s. In *BWR*s the various types of oxidation kinetic are shown in Figure 1-3.

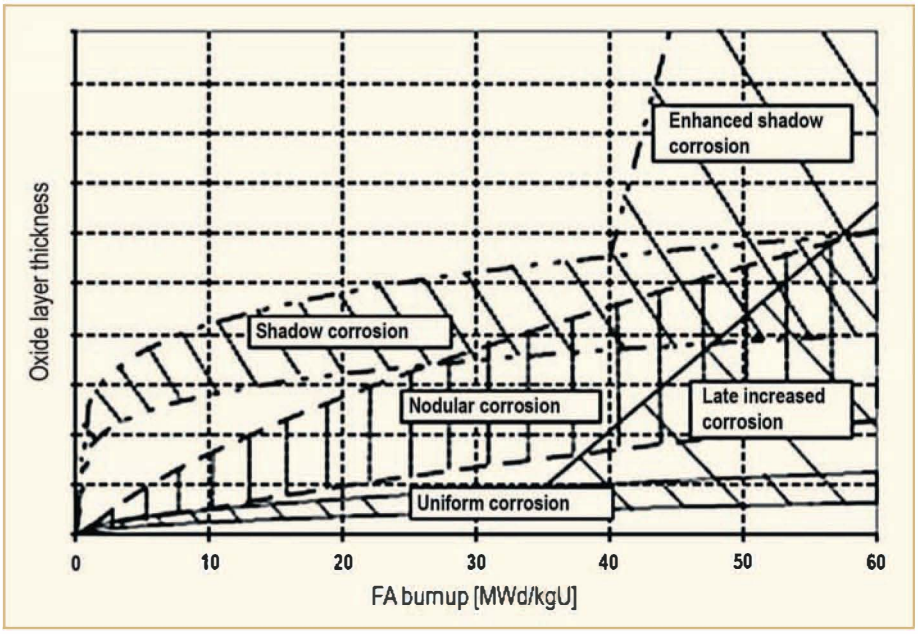

Figure 1-3: Characteristics of different types of corrosion observed in *BWR*s. Oxide layer thickness in arbitrary units versus fuel assembly burnup, *ZIRAT7 STR* "Corrosion of Zirconium Alloys".

Uniform corrosion continues at a very low rate out to high burn-ups. During reactor exposure the microstructure of the Zircaloys used in *BWR*s is continually evolving due to irradiation damage and *SPP* dissolution. In the range 30-50 MWd/kgU (6-10x10^{21} n/cm^2, E>1 MeV), changes in the microstructure induce an acceleration of uniform corrosion, as described in Section 4. First, patches of white oxide appear in the otherwise black or grey uniform background, as illustrated in Figure 1-4. These patches remain very thin, about the same

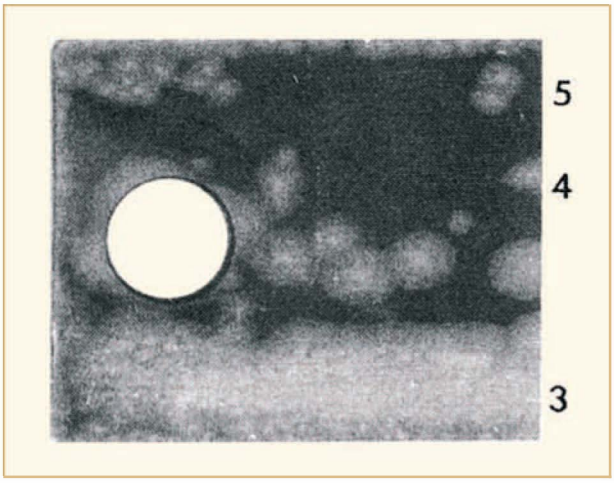

Figure 1-4: Patch oxide formation on Zircaloy-2 after an exposure of 8.5x10^{21} n/cm2, E> 1 MeV. The oxide is thinnest at uniform black oxide (5) and patch oxide (4), and is thickest at coalesced patches (3), Huang et al., 1996.

as the black uniform corrosion film. At some point the patches cover 100% of the surface and oxide thickening occurs at an accelerated rate, labeled "late increased corrosion" in Figure 1-3.

Importantly, at the same or somewhat higher fluences, a marked increase in hydrogen pick-up fraction occurs. This hydriding is potentially a more serious issue than the corrosion increase.

Figure 1-5 gives optical micrographs and schematics of various types of corrosion. Schematics A and C show normal and increased uniform oxide, and the others illustrate nodular corrosion. Zr-Nb alloys and small-*SPP* Zircaloys (average *SPP* size less than about 0.1 μm) in general do not

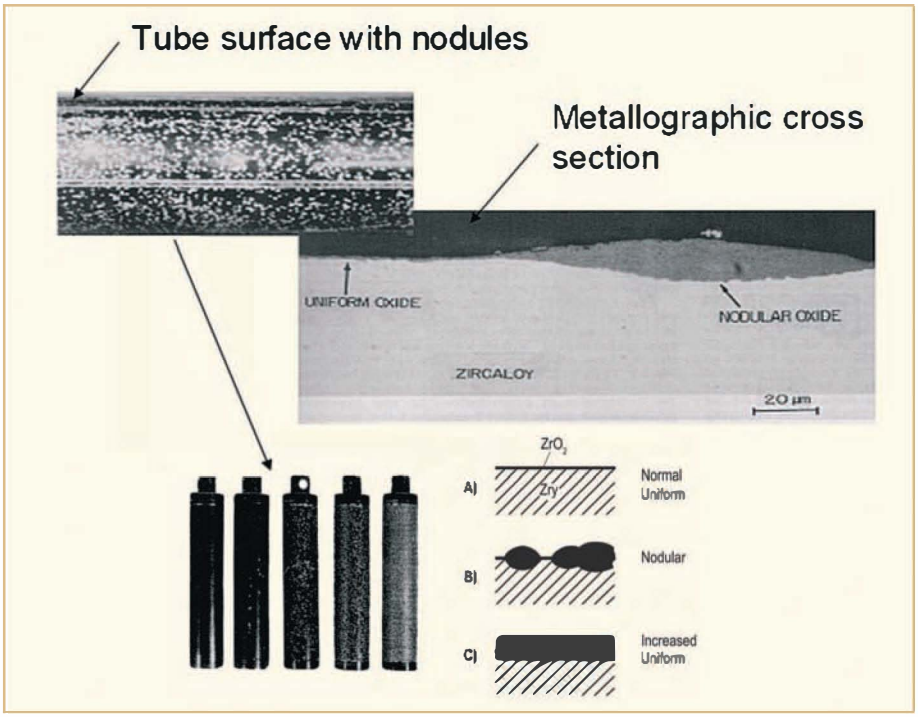

Figure 1-5: Corrosion morphology for Zircaloy in *BWR*s.

form nodules. In large-*SPP* Zircaloys, nodules initiate early in life and grow at a decreasing rate with fluence. In some cases, for aggressive water chemistries and susceptible material, nodules can coalesce to cover the entire surface. Nodular oxide thickness does not generally cause performance problems; however in severe cases spalled oxide can be a source of "grit" in control drive mechanisms. Serious fuel failure problems can be induced by a combination of heavy nodular corrosion and copper-zinc-laden crud, resulting in the Chalk River Unidentified Deposits (*CRUD*) Induced Localized Corrosion (*CILC*) phenomena discussed in Section 4.

Susceptibility of Zircaloys to in-reactor nodular corrosion can be identified by laboratory high temperature steam tests. The most effective testing procedures are variations of the "two-step test" described by Cheng et al., 1987 where Zircaloys are exposed to steam at 410°C/1500 psi (683K/102 bars) for 8h followed by 510°/1500 psi (783K/102 bars) for 16h. In such tests, Zr-Nb alloys do not exhibit nodular corrosion.

The fifth type of corrosion, indicated in Figure 1-3, is the so-called shadow corrosion, described in more detail in Section 4. Shadow corrosion is induced on all zirconium alloys when they are in close proximity to many non-zirconium alloys such as stainless steel or Inconel. The oxide thickness is unusually large and often appears to be particularly dense and un-cracked. For example shadow corrosion oxide induced by a stainless steel control blade bundle is shown in Figure 1-6. Shadow corrosion has "always" been present in *BWR*s, but not in *PWR*s, primarily

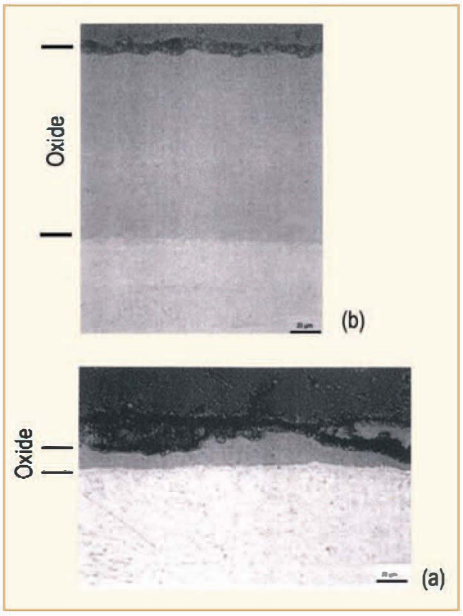

Figure 1-6: Zirconium oxides near (b) and away from (a) a stainless steel control blade bundle, Adamson et al., 2000.

related to the high *PWR* hydrogen concentration which reduces or eliminates galvanic potentials between dissimilar alloy components. In *BWR*s shadow corrosion caused no performance issues until recently when at one reactor fuel failures were induced by unusually severe "enhanced spacer shadow corrosion", Zwicky et al., 2000. More recently, shadow corrosion has been alleged to be involved in *BWR* channel bow problems, Mahmood et al., 2007. Both issues are addressed in Section 4.

The following sections of this *STR* will address in more detail the mechanisms which are believed to be most important in describing corrosion in zirconium alloys.

1.1 Effect of temperature (Alfred Strasser and Peter Rudling)

1.1.1 Introduction

Temperature is one of the most important parameters affecting zirconium alloy cladding corrosion. Yet it is a parameter that can not be measured directly --- it can only be calculated. Uncertainties in the calculations, or modeling, are the results of uncertainties contributed by numerous other parameters that are necessary components of the models, some of which are equally difficult to measure. *Knowledge of the parameters that affect the temperature and an appreciation of the uncertainties related to each parameter are important in the evaluation of the relationship of temperature to in-reactor corrosion.*

Temperature measurements of samples in ex-reactor tests or some test-reactor tests (particularly of unfueled samples) can be made reasonably reliably. *The objective of this section is to identify the various parameters that affect the temperature of cladding during in-reactor service, note their degree of importance and provide the reader with some feeling of the uncertainties involved.*

Ex-reactor corrosion tests of zirconium alloys with initially clean surfaces provide the data that show the dramatic increase of corrosion with temperature. In an example of work by Bettis Labs. shown in Figure 1-7, a 26% increase in weight gain was produced as a result of a 5°C increase in temperature in a nearly 7-year-long test at a typical cladding temperature of 335°C. The "typical" maximum cladding temperatures are summarised in Table 1-3 for *BWR*s and *PWR*s along with the reactor inlet and outlet coolant temperature ranges. The cladding temperatures are calculated numbers for clean surface cladding at nominal reactor operating conditions.

Table 1-3: Light Water Reactor *(LWR)* Coolant and Cladding Temperatures, Nuclear Engineering International, 1998.

	BWR	*PWR*	*VVER*-440
Coolant Inlet Range			
°C	272-278	279-290	267
°F	522-532	534-554	513
Coolant Outlet Range			
°C	280-300	313-330	296-300
°F	536-572	595-626	565-572
Max. Clad Temperature			
°C	310-320	318-360	335-345
°F	590-608	604-680	635-653

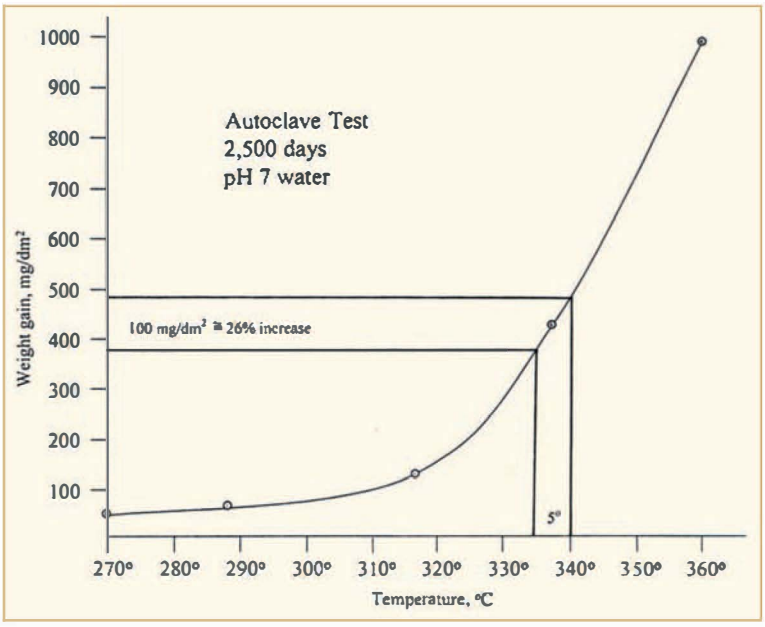

Figure 1-7: Zircaloy-2 and 4 weight gain as a function of temperature, Hillner et al., 2000.

The lower pressure and the boiling regime of *BWR*s limit their coolant temperatures and inlet-to-outlet temperature ranges compared to *PWR*s. Greater flexibility in *PWR*s also permitted them to increase coolant outlet temperatures (and peak cladding temperatures as a result) for the more modern units in their race to increase efficiency and lower the predicted fuel cycle costs. It is interesting to note that, due to the high corrosion rate of cladding at the high temperatures, many of these newer *PWR*s have modified their system to reduce temperatures and lengthen the life of their fuel cladding.

The Russian *VVER* 1000 units fall within the temperature range of the western *PWR*s, but the *VVER* 440 units are lower in temperature and are shown separately for that reason.

A brief overview of the relationship of *PWR* coolant temperatures and cladding corrosion is given in Table 1-4. At an exposure of 45-48 GWd/T the oxide thickness on Zircaloy-4 claddings range 11-37 μm in the lowest-coolant-temperature early *PWR* (Ginna) to 78-120 μm in one of the more recent, high-temperature plants (Gösgen), by a factor of about 4. The other plants cited are in a range of coolant temperatures and oxidation levels between these two extremes.

Table 1-4: Corrosion of Standard Zircaloy-4 as a Function of Plant Parameters, *IAEA*-TECDOC-996, 1998.

Plant	Ave. Core kw/lit.	Ave. Core Outlet °C (°F)	Oxide Thickness, μm	Burn-up-GWd/mtU	
				Rod	Assy
Ginna	89	317 (602)	11-37	45-48	42.5
			20-41	54-56	52
ANO-2	97	323 (613)		58 (ave.)	52
			21-73	57-60	
			40-80	60-64	
Grohnde	95	327 (602)	82-92	45-46	
Summer	105	327 (620)	76-86	46-48	46
North Anna	109	327 (620)	52-96	44-47	46.4
Gösgen	101	325 (618)	78-120	40-48	

The temperature at the interface between the zirconium alloy metal surface and the zirconium oxide formed governs the post-transition corrosion rate and can be formulated as:

$$\frac{\Delta S}{\Delta t} = C_2 \exp(-Q_2 / RT)$$

where

S is the oxide thickness
t is the time
Q_2 is the post-transition activation energy
C_2 is an irradiation corrosion enhancement factor
R is the Gas Constant
T is the temperature at the metal/oxide interface

The C_2 constant is very different for zirconium alloys in *BWRs* and *PWRs*. Experiments (see e.g. Stehle et al., 1984) comparing the out-of-pile with the *PWR* corrosion rates have suggested a value of C_2 = 2 to5, while similar tests for *BWRs* have indicated a C_2 constant that varies with temperature. At temperatures of 200°C, C_2 = 1000, while at 400°C the C_2 =1. Thus, the out-of-pile and in-pile corrosion rates for Zircaloy can be schematically shown as in Figure 1-8. *The bottom line is that a temperature increase at the metal/oxide interface (below a maximum temperature of 400°C) results in a larger increase of the corrosion rate in a PWR than in a BWR. This is the reason that there is a licensing limit on the maximum oxide thicknes for fuel rods in PWRs but not in BWRs. Since the oxide has a lower thermal conductivity than that of the metal a large oxide thickness increase may increase the metal/oxide temperature and thereby increase the corrosion rate in a PWR leading to a thermal feedback effect.*

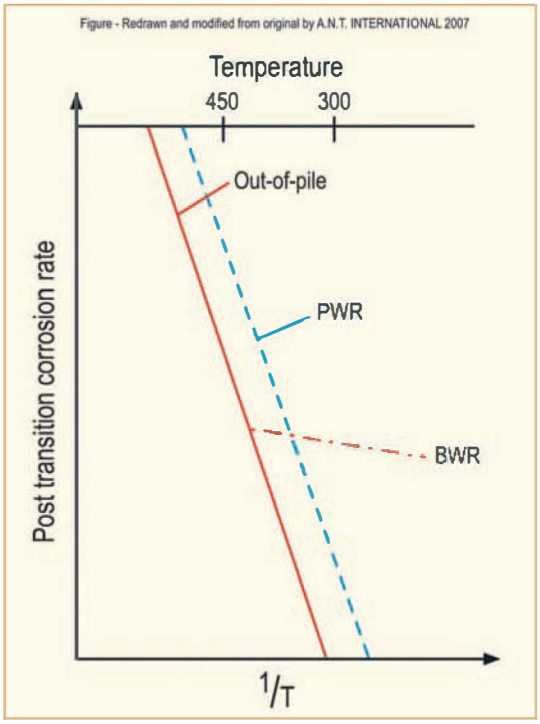

Figure 1-8: Schematic diagram showing the impact of metal/oxide interface temperature on post-transition corrosion rate.

Figures 1-9 and 1-10 depict typical *PWR* fuel clad temperatures and the resulting fuel rod axial oxide thickness profile. Higher corrosion rates occur in the upper part of the fuel rod, due to higher temperatures at the oxide/metal interface. The fuel rod oxide thickness suppression at the grid locations is due to lower fuel clad temperatures at these locations. This is caused by:

1) increased turbulence due to the spacer resulting in better cooling and
2) lower reactivity due to parasitic thermal neutron absorption of the grid material

However, it is important to note that the *PWR* corrosion acceleration, due to thermal feedback effect, occurs at a much larger oxide thickness (about 100 μm) than the corrosion acceleration due to hydride formation, see Figure 1-1.

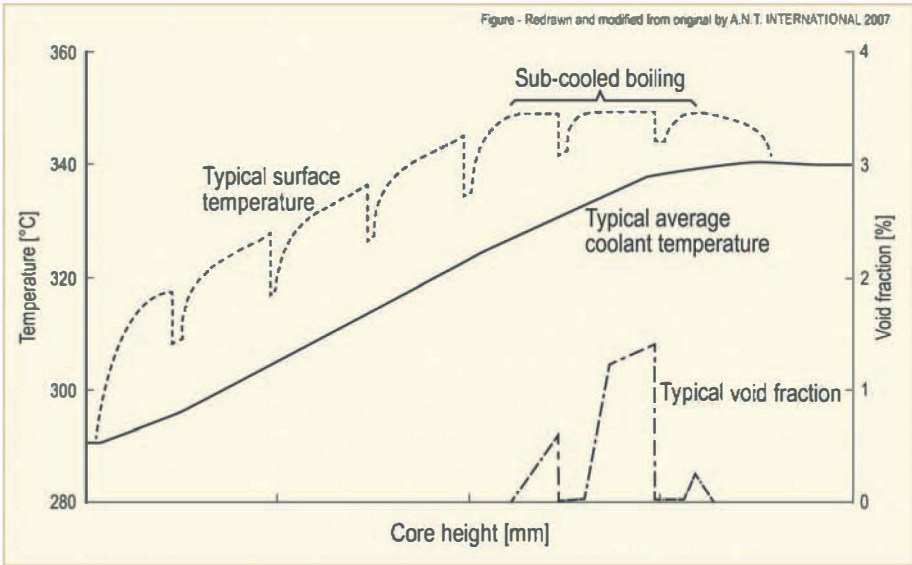

Figure 1-9: Schematics showing typical *PWR* fuel clad surface temperature as well as bulk coolant temperature as a function of fuel rod elevation. In the upper part of the fuel rod, the coolant temperature may locally at the fuel rod surface exceed the saturation temperature leading to local boiling (called "sub-cooled boiling" since the bulk coolant temperature is below the saturation temperature).

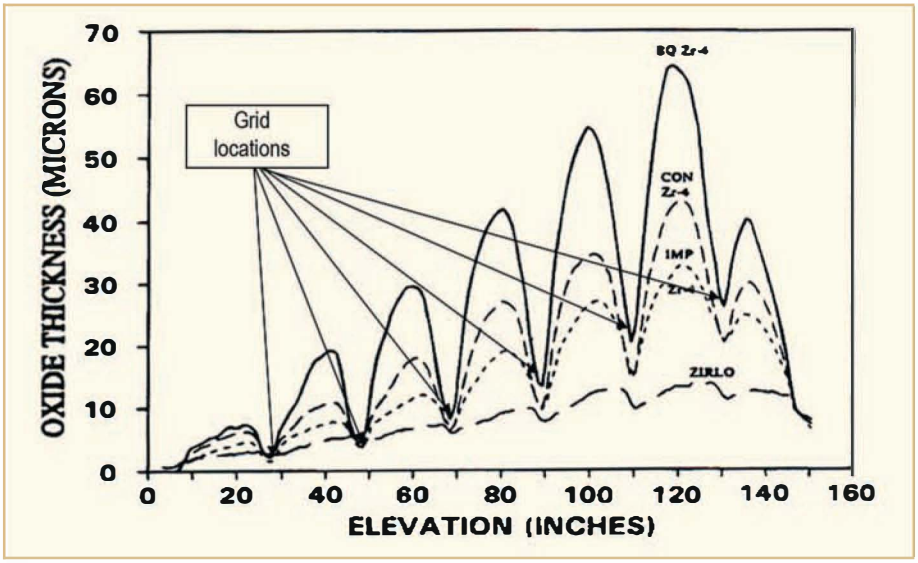

Figure 1-10: *PWR* in-pile oxide profile. Modified figure according to Sabol et al., 1994.

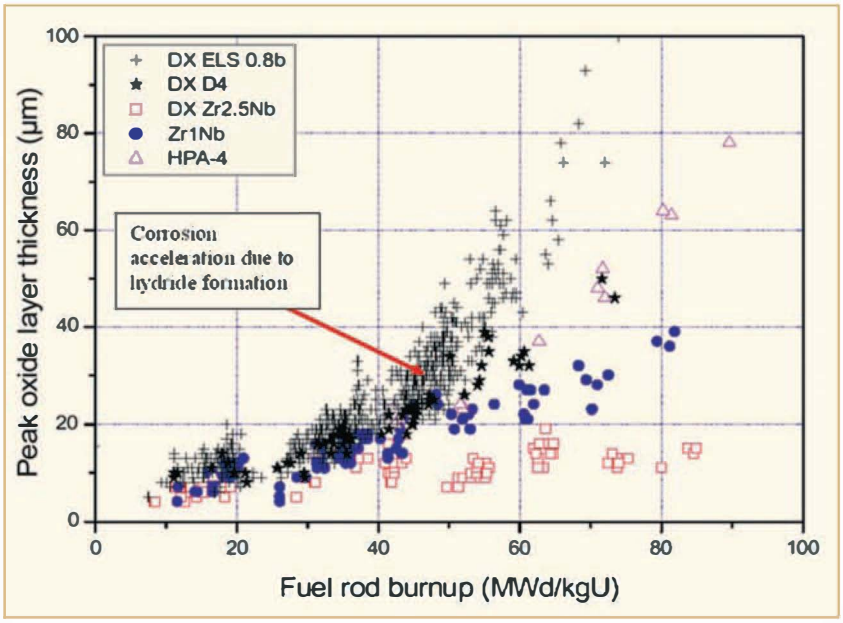

Figure 1-11: Siemens *PWR* data. Modified figure according to Seibold et al., 2000.

In *BWR*s the coolant and fuel rod temperature axial profiles are much more constant than that of the *PWR*s. The more constant axial temperature in the *BWR*s is due to the boiling that occurs at about the lowest spacer location. The fuel rod oxide profile is NOT correlated to the fuel rod temperature (except in those cases when the fuel rod is overheated - temperatures ranging from 400C and upwards - due to a thermally insulating *CRUD* layer), see Section 4.4.

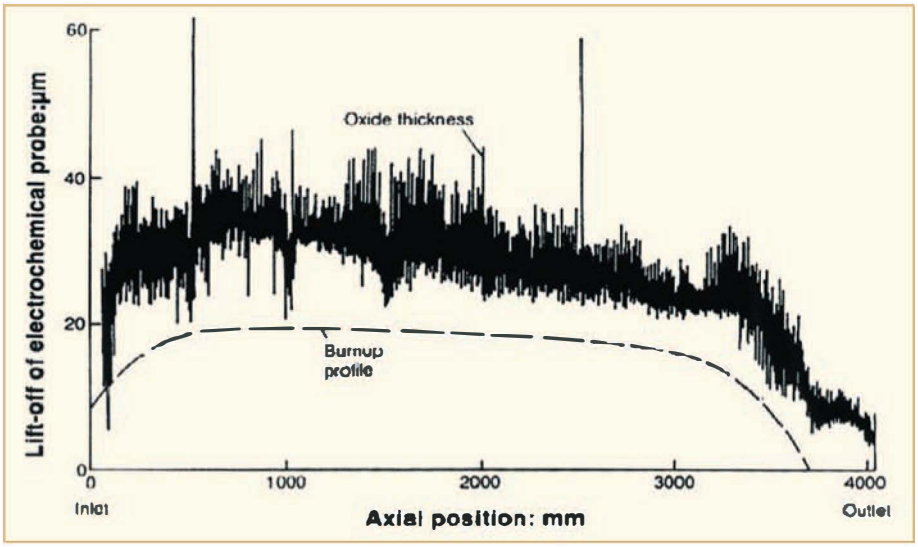

Figure 1-12: *BWR* In-pile Oxide Profile, Garzarolli et al., 1979.

The variables that determine the temperature at the metal/oxide interface are shown pictorially in Figure 1-13 and are listed in Table 1-5. As shown on the figure, the interface temperature in question is determined by the power or heat flux (Q) generated in the fuel rod and the efficiency of the coolant in removing this heat. The thermal resistance of the oxide and the crud layers between the coolant and the metal surface need to be taken into account in the calculation of the metal oxide interface temperature.

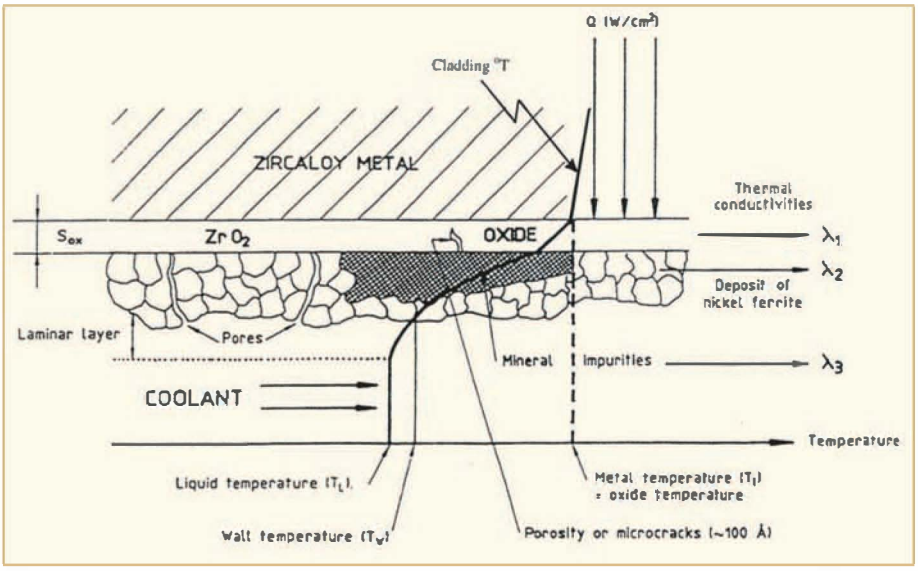

Figure 1-13: Factors that affect cladding temperature, *IAEA*-TECDOC-996, 1998.

Table 1-5: Variables in Determining Metal-Oxide Interface Temperature

- Bulk fluid °T
- Laminar boundary layer

  Single phase

  – bulk fluid °T
  – heat flux
  – heat transfer coefficient (Dittus-Boelter, etc.)
    - hydraulic diameter
    - fluid properties: density, viscosity, specific heat, thermal conductivity, velocity
    - Nusselt number

  Two phase

  – ditto, but for nucleate boiling
    Wall °T = $^{\circ}T_{saturation}$ + $^{\circ}T_{wall}$
  – heat transfer correlation (Jens-Lottes, Thom, Chen, etc.): heat flux, pressure
- *CRUD* layer
  – heat flux
  – crud-bulk fluid interface °T
  – crud thickness
  – crud thermal conductivity
- Oxide layer
  – heat flux
  – oxide-crud interface °T
  – oxide thickness
  – oxide thermal conductivity

The thermal-hydraulics of the coolant and the thermal properties of the metal are reasonably well known. The crud thermal characteristics are the least well-characterized and the difference between the deposits observed after shutdown and those present during operation are also not always known with certainty.

The heat flux, or power, generated in the fuel rod is a key parameter in each one of the variables that affect the metal/oxide interface temperature as listed in Table 1-5. The temperature gradient produced by the heat flux increases with the increased thermal resistance (decreased thermal conductivity) of the material it passes through. The resulting increased temperature increases corrosion rate. The effect of heat flux alone on the corrosion rate is difficult to assess because other parameters are invariably involved as well. The heat flux can cause secondary effects that increase corrosion rate. As an example, corrosion resistance can be lowered due to the presence of hydride surface layers on the cladding. Also, increased subcooled boiling at the *PWR* fuel rod surface may enrich water-soluble species in the zirconium oxide that potentially could result in degradation of the oxide protectiveness.

Different fuel rod power histories can affect the oxidation rates in different manners. In this case, the effects are interactive with the oxide and possibly the crud thickness as these develop with exposure. An example of a theoretical, calculated case is given below.

The power histories for a Low Leakage (*LL*) fuel management scheme by a *PWR* vendor are compared to his out-in scheme (*OI*) at the same exposure, Figure 1-14. The high power early in life in the *LL* scheme is advantageous from an oxidation perspective, since then the oxide layer is thin, the interface temperature is low and in addition the corrosion rate is low. The *OI* scheme experiences higher power at the end of life when the oxide thickness/interface temperature is higher, the oxidation rates and the resulting increases in oxide thickness are greater. The comparison of oxide thickness shown in Figure 1-14 indicates a corresponding higher peak oxide thickness at end-of-life of the *OI* scheme, Strasser et al., 1993.

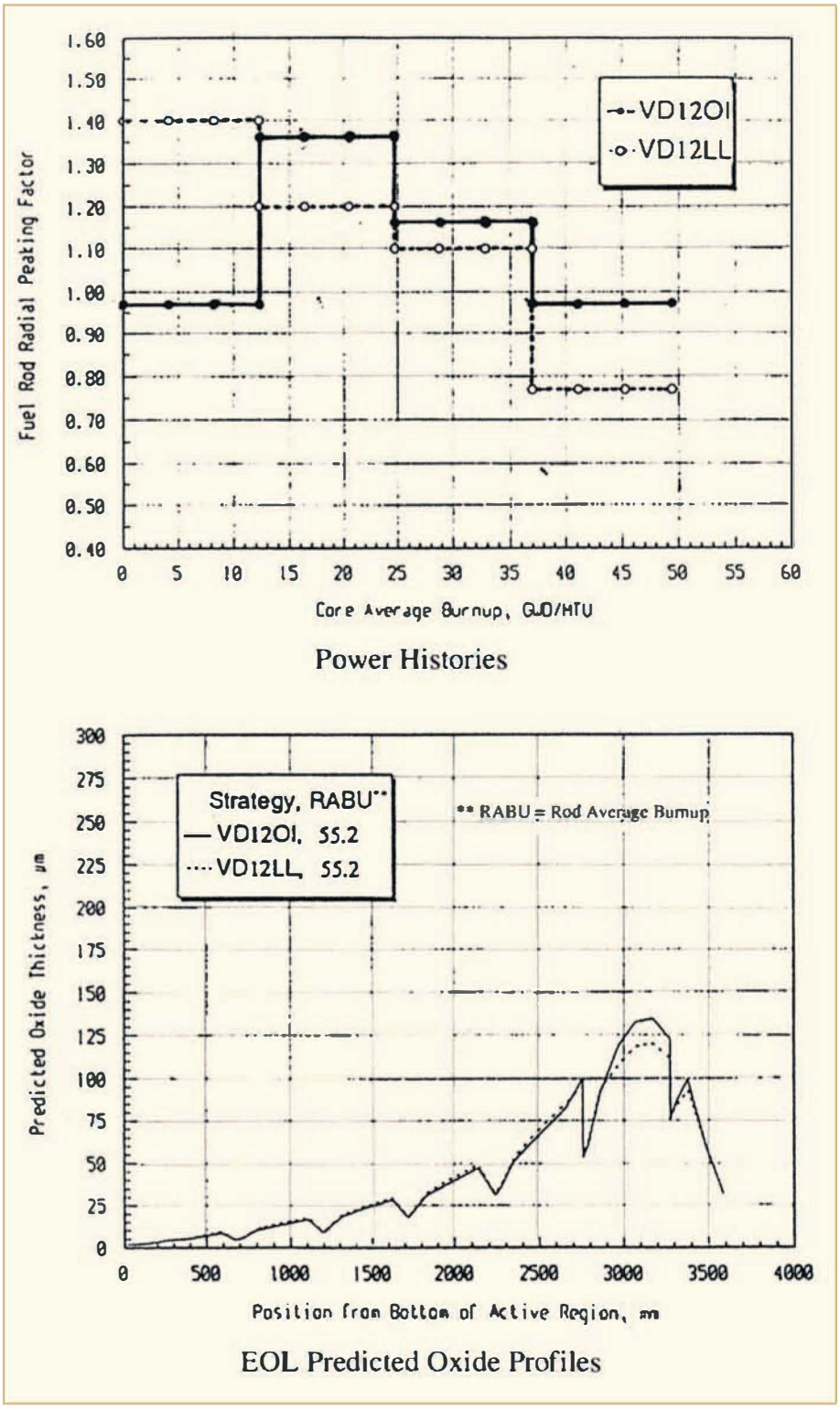

Figure 1-14: Comparison of the effects of out-in (VD12*OI*) and low-leakage (VD12*LL*) fuel management schemes on *PWR* cladding oxidation, Strasser et al., 1993.

Properties of zirconium oxide and *CRUD* deposits

The temperature of the oxide-metal interface can be calculated from the relationship:

$$T = T_w + \Phi (S/K) \qquad \text{where,}$$

T = temperature of the oxide/metal inteface (Kelvin)
T_w = temperature of the oxide/water interface (this assumes no crud) (Kelvin)
Φ = heat flux (W/m²)
K = oxide thermal conductivity (W/m K)
S = oxide thickness (m)

The heat flux and the oxide thermal conductivity are key parameters in determining the interface temperature. Figure 1-15 compares some of the unirradiated and irradiated ZrO_2 thermal conductivity data and Table 6.9 on Page 168 of *IAEA*-TECDOC-996, 1998, gives an additional, extensive database with a wide range of values. The actual values of K used by modelers are in the range 0.8 – 2.0 W/m K, which is quite wide. The temperature drop across a 70μm oxide layer with a heat flux of 70 W/cm² is 31°C using a K of 1.8 and 70°C with a K of 0.8. *The difference in K can cause a 4X increase in post-transition corrosion rates in some predictive models.*

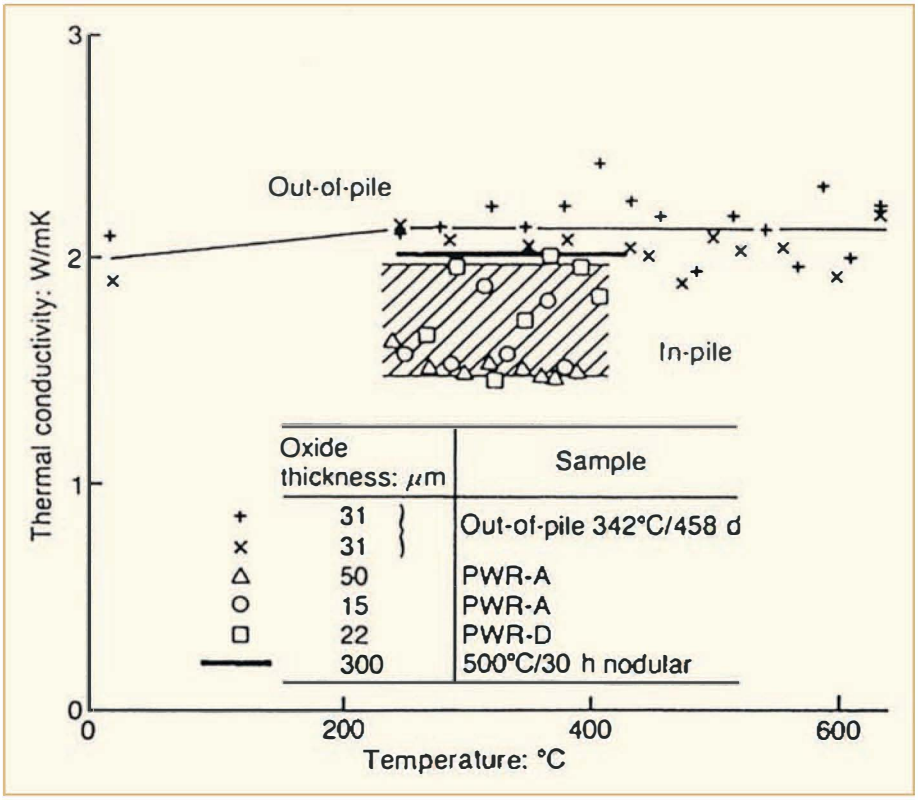

Figure 1-15: ZrO_2 Thermal Conductivity, Stehle et al., 1984.

A comparison of predicted oxide thickness as a function of time using a smaller difference in thermal conductivity of 1.2 and 1.8 is shown in Figure 1-16. This can still result in significant differences in oxidation predictions for high burn-up performance.

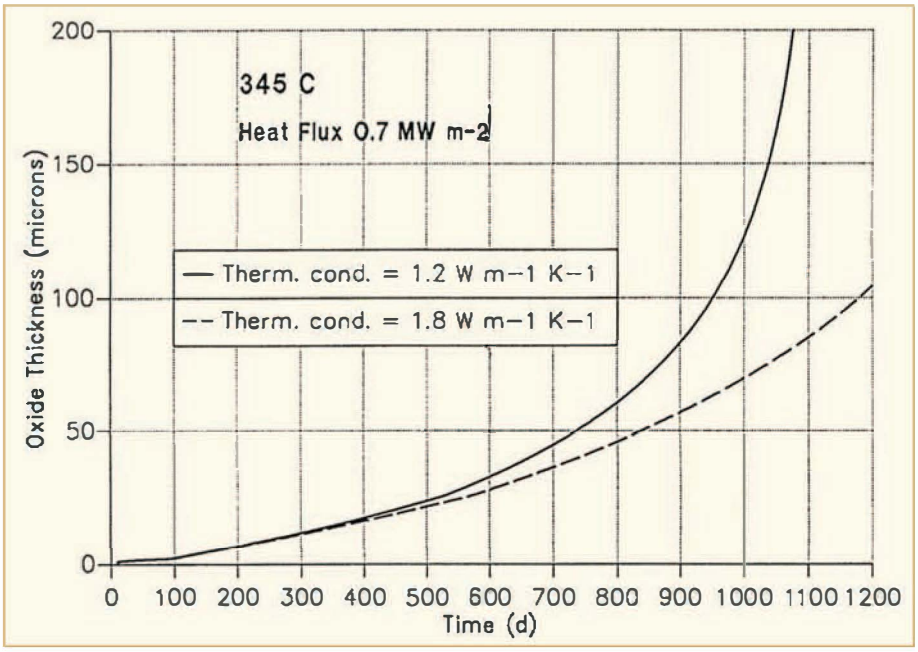

Figure 1-16: Example of effect of different oxide thermal conductivity values on predicted oxide thicknesses (Nuclear Electric – ZIRC Code predictions), *IAEA*-TECDOC-996, 1998.

The thermal conductivity of irradiated ZrO_2 is slightly lower than that of the unirradiated oxide. Other changes in the conductivity value could be induced by penetration of the porosity by the coolant and its components, cracking and spalling. These added uncertainties will be magnified as thick oxide films are developed at extended burn-up or on materials with poor oxidation resistance to the coolant conditions.

The sources of crud on the fuel are the corrosion products from the reactor primary coolant system that deposit primarily on the hot heat transfer surfaces i.e. the fuel cladding. *The effect of crud deposits on the cladding metal-oxide interface temperature are subject to even greater uncertainties than the effect of the oxide layer, because the crud can be present in a wide variety of morphologies.* The crud layers can have physical structures that vary from dense layers to porous ones. The porous layer types can vary as well and be fluffy, loose deposits; dense structures with pores and cracks or relatively loose deposits with convective coolant chimneys (wicks). Each of these forms will have a different thermal conductivity. The conductivity of these heterogeneous deposits depend partly on the crud composition and structure and partly on the composition and thermal state of the coolant that penetrates its voids.

The measurement of the thermal conductivity of the crud layers, particularly the loose or non-adherent ones, is extremely difficult since the preservation of the layers for subsequent measurement may not be possible. A further, more basic question is what the crud layer was during operation and whether the crud deposited on the fuel during shutdown; this question applies primarily to the loose crud types. Examples of crud thermal conductivity measurements and estimates are shown in Table 1-6 and are compared to the thermal conductivities of water and steam that can infiltrate the crud. The conductivity of the various crud compositions is generally higher than that of ZrO_2, higher than that of water and significantly higher than steam -- - that's the good news; unfortunately the variability and uncertainty among the various crud types is greater.

Table 1-6: Thermal Conductivity of *CRUD* Deposits on Fuel Cladding, Wikmark & Cox, 2001.

Layer	Thermal Conductivity $W \cdot m^{-1} \cdot K^{-1}$	Remark
Water	0.57	288°C, 7MPa
Steam	0.063	288°C, 7MPa
"Porous magnetite crud"	1	~ 90% density
Porous hematite crud	>6	~ 10% density
PWR zinc crud	1.1	At 350°C
CuO	3.3	At 15°C
Compressed hematite	0.5	At 100°C
Dense copper-iron crud	2	At 220°C

The "normal" crud that results from normal reactor operation rarely results in excessive cladding temperatures and the increased corrosion observed is due to a combination of increased metal/oxide? temperature and Li concentration that is increased significantly above its nominal level in the coolant within the crud and the oxide film.

Impurities such as Al, Ca, Mg, Mn and Si tend to densify the crud and have the potential to raise the cladding temperature as shown in early ex-reactor experiments, Figure 1-17 and confirmed by fuel failures due to such crud in the Steam Generating Heavy Water Reactor (*SGHWR*) in the UK. Since then, no adverse effects have been identified in-reactor to date although recommendations are to keep these impurities at a low level in the coolant. Measuring the effect of crud on cladding temperature has been and and is a current topic of investigations in the CIRENE loop in Cadarache, France.

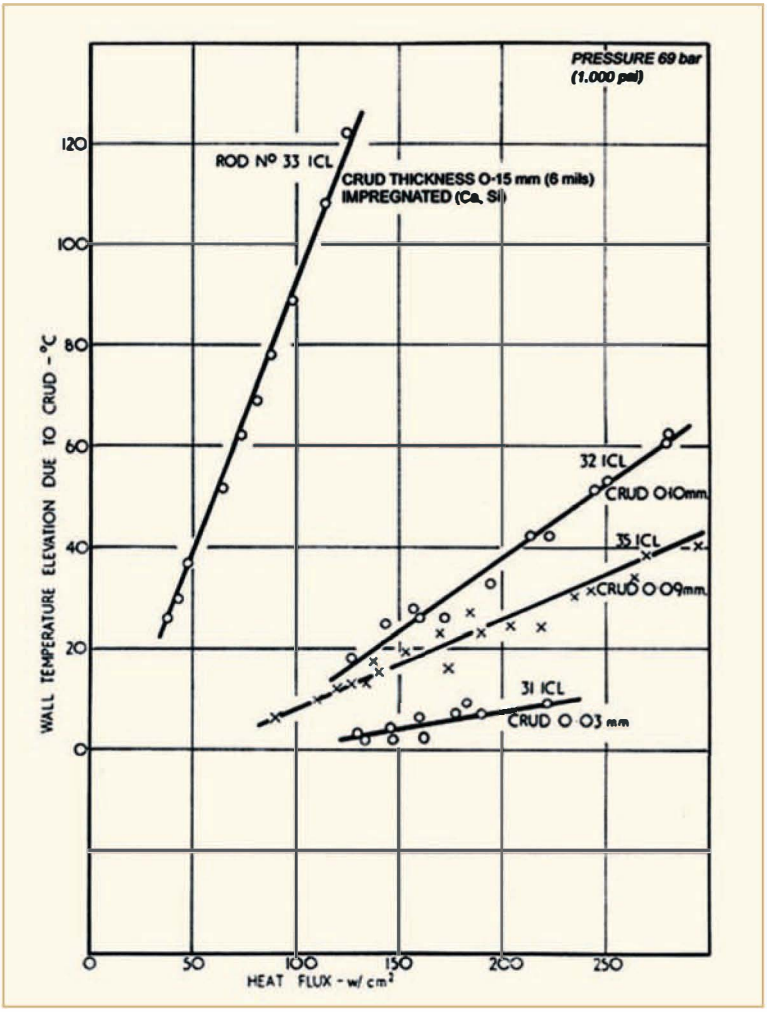

Figure 1-17: The effect of magnetite crud on maximum wall temperature elevations, Macbeth et al., 1971.

The injection of Zn for the reduction of activity transport or steam generator tubing corrosion has resulted in the formation of zinc ferrites in a thin, dense layer. A small, but to date non-detrimental increase in corrosion has been noted due to the resulting temperature increase.

Heavy crud deposits that raise the interface temperatures significantly can result in fuel failures, see Section 4.4.

As an example a heat flux of 120 W/cm², about the maximum for *BWR*s, the effect of thermal conductivity is as follows:

1) a 100μm-thick crud layer with a conductivity of 2 W/m °C raises the clad temperature by 60°C,

2) a 15μm steam-filled crack with a conductivity of 0.07 W/m °C raises it by 258°C.

The small steam gap would raise the nominal 295°C clad surface temperature to over 550°C. Oxidation at this temperature level would fail the clad in significantly less than 100 days. At 600-650°C the clad would fail in less than 5 days.

Thermal Hydraulics. The temperature of the coolant entering the bottom of a reactor core is uniform and increases as it passes through the core as a function of core power and coolant flow rate. For example, an increase in the coolant inlet temperature in a *PWR* will result in higher fuel rod temperatures that in turn can increase corrosion rate.

2 Basics of the corrosion and hydrogen pick-up process (Brian Cox)

2.1 Initial zirconium surface condition

Zirconium and its alloys are highly reactive metals and in oxygen containing atmospheres always have at least a thin oxide film on their surfaces, Cox, 1976. This film can be dissolved in a mixture of HNO_3/*HF* (High Frequency) during electropolishing, but will always reform when the metal is exposed to air or water at Room Temperature (*RT*). Hence its description as the "air-formed oxide film". This film can also be removed by dissolution into the metal by heating at high temperature in a vacuum (or near vacuum). This occurs because oxygen is more stable thermodynamically when present as a dilute solution in the metal than it is as a ZrO_2 surface film.

At intermediate temperatures (> ~200°C) the air-formed oxide will increase in thickness as a result of oxygen diffusion through the air-formed oxide to produce more layers of ZrO_2 at the oxide metal interface. If the oxidation environment is water then water molecules are dissociated at the oxide/environment interface by the electrons from the oxidation process diffusing out (in the opposite direction to the oxygen ions diffusing in). The hydrogen atoms resulting from this process may recombine to form hydrogen molecules in solution in the water but some of them may manage to diffuse into the metal (see hydrogen uptake mechanism later). However, there is no evidence that hydrogen in the atomic form can diffuse through the ZrO_2 crystal lattice. The only mobile species in the oxide film at normal reactor operating temperatures are oxygen ions/oxygen ion vacancies and electrons/electron holes.

2.2 Galvanic processes

The oxidation process should be considered as an electrochemical cell reaction. Figure 2-1, Cox, 2003 and 2005.

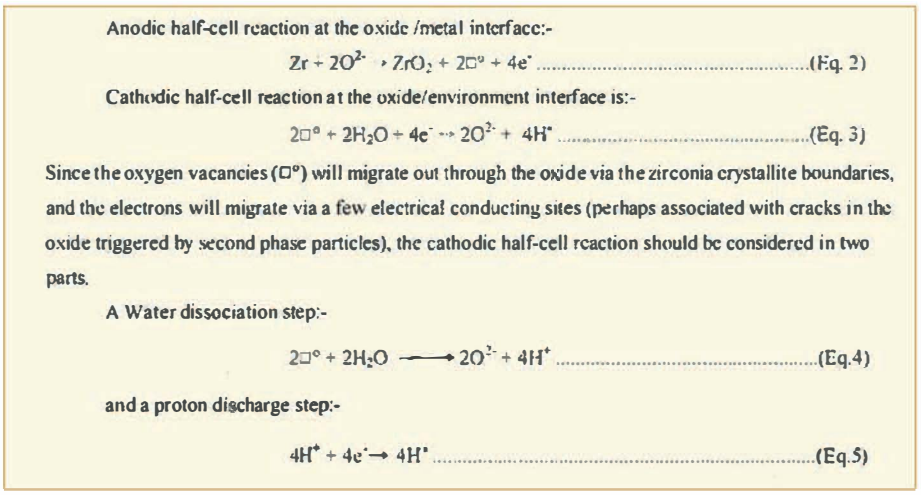

Figure 2-1: "Corrosion as an Electrochemical Process".

The oxygen vacancies will diffuse out from the oxide/metal interface in the opposite direction to the oxygen ions, which have been shown to diffuse preferentially via the oxide-crystallite boundaries, Cox & Roy, 1966; Cox & Pemsler, 1968. The hydrogen atoms released at the oxide/environment interface by reduction by the electrons can recombine to form hydrogen molecules (which will dissolve in the water) or can diffuse inwards to the oxide/metal interface if they can find a suitable path through the oxide film. The direct diffusion route through the oxide film is not available to them, since all claims to measure such diffusion coefficients have been shown to be due to OH^- ions migrating down cracks or pores in the oxide and were not H^0 diffusion through the ZrO_2 Lattice, Ramasubramanian, 1996 and Elmoselhi et al., 1994. We will go into more details about this process, since the proportion of hydrogen atoms successfully diffusing into the metal gives the value for the "Hydrogen Pick-Up Fraction*".

2.3 Rate-determining step for zirconium oxidation

Only in a very few conditions, far removed from those in an operating reactor has Zr^{4+} migration in the oxide been observed. In the range of normal reactor operating conditions there are only two mobile species in the ZrO_2 lattice: oxygen ions/vacancies and electrons/holes. Although oxygen diffusion is a slow process, it is the essential mechanism by which the oxide thickens. The migration of electrons is even slower. Zirconia films are better insulators than they are oxygen diffusion barriers. The only competitor in the electrical insulator field is hafnium oxide, and both are being considered as insulators in micro- electronic devices because of their excellent resistivity and high band-gaps (4-5 eV).

Because of this very high electron resistivity electron transport and not oxygen ion diffusion is the rate determining step in the zirconium oxidation process. This fact has been demonstrated many times by the measurement of the electrical potential that develops across the oxide film during corrosion. The potential of the oxide/metal interface relative to the potential of the oxide/environment surface can be measured in any non-aqueous environment (surface potentials confuse the measurement technique in water but it can be measured in dry steam, oxygen, air and fused salts. The results are always the same: the oxide/metal interface rapidly develops a negative potential after oxidation starts. The potential increases ~- 1.1 to -1.2 V, roughly equal to the half-cell electrochemical potential. Such a negative potential develops to accelerate the electron migration process and retard the oxygen-ion diffusion process, until both processes operate at the same rate and further increases in space charges cease, Figure 2-2, Bradhurst et al., 1965. Thus, the electron transport is the more difficult process since it needs an accelerating potential to equalise the two processes. Since the rate controlling process is not oxygen ion diffusion through the ZrO_2 lattice, the pre-transition corrosion kinetics are not parabolic. Electron conduction-the rate determining step parabolic obeys either Poole-Frenkel or Mott-Schottky kinetics, which tends to give kinetics nearer to a cubic, but they can vary over quite a range of exponents.

* *HPUF*

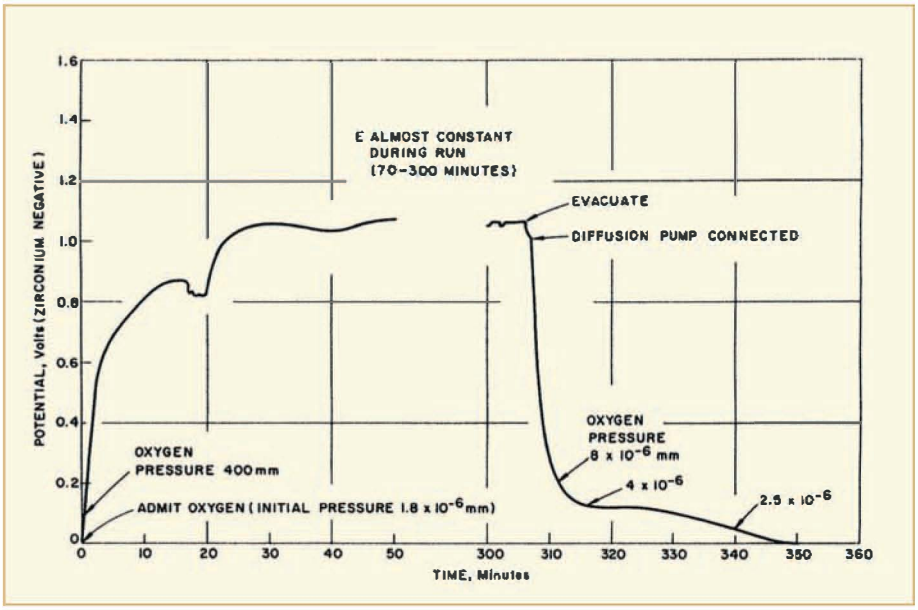

Figure 2-2 Behaviour of potential developed during oxidation of zirconium at 700°C.

Suggestions that the rates of the surface reactions are rate controlling, Bossis et al., 2000, do not bear inspection, since the initial growth rates of oxide films in oxygen, air, steam, water, H_2SO_4 (<0.5 molar), HNO_3 (<0.5 molar), NH_4OH, and even LiOH (< 0.1 molar) are all nearly identical at temperatures in the 300-350°C range. The big differences between these environments only appear when the oxide films' protective layers begin to break down (see later). The rates of surface reactions in this wide range of environments must vary by many orders of magnitude. Arguments for rate control by the rate of the surface reaction usually arise because the authors have chosen to ignore the cathodic half-cell reaction (i.e. electron transport).

2.4 Structural growth of zirconia films

The initial "air-formed" oxide present on all Zr alloy surfaces exposed to an oxygen-containing environment, consists of an array of roughly equiaxed nano-crystals of ZrO_2, with many different orientations relative to the orientation of the Zr grain on which they form. These crystallites are ~ 2 nm diameter and are either cubic or tetragonal (*t*) zirconia, Ploc, 1970. It is very difficult to strip and determine the crystallography of these crystallites without doubts, Ploc, 1968 and 1969. Such a determination may not be important for the structure of thicker oxides. At elevated temperatures some of these crystal orientations grow preferentially to develop into arrays of columnar crystallites. 'The preferential crystallite orientations are those that will minimise stress due to the volume change on going from Zr to ZrO_2 (the Pilling-Bedworth ratio of ~1.56).

The result is an oxide film formed of columnar ZrO_2 grains with a preferred orientation, Figure 2-3, Yilmazbayhan et al., 2006. The extent to which these columnar crystallites grow without breaking down is a function of the alloy composition and the oxidation environment. Adjacent to the oxide/metal interface, where new oxide is forming, there is usually a layer of tetragonal ZrO_2 crystallites. This has been established by Raman Spectroscopic studies of the oxide, Godlewski et al., 2000. At the oxide/environment interface these crystallites transform to monoclinic (*m*)-zirconia. This *t*-->*m*-zirconia transformation will have inevitably generated micro-cracks in the oxide because of the volume change associated with the phase change. Possible mechanisms for this transformation will be discussed later (see Section 2.7).

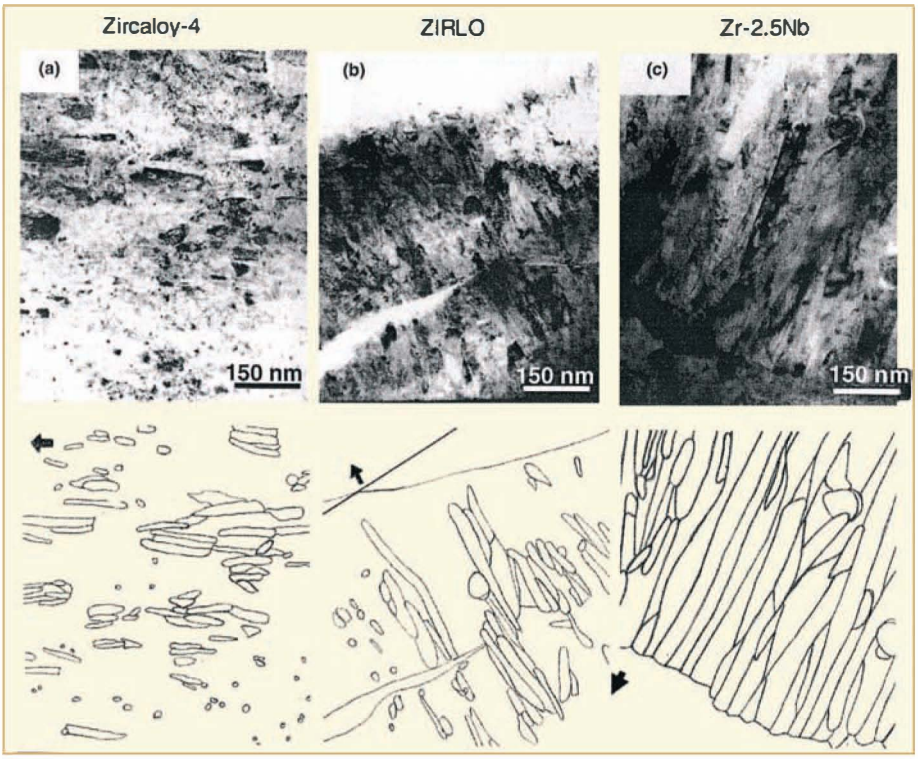

Figure 2-3: Differences in extent of columnar oxide crystallite formation, Yilmazbayhan et al., 2006.

The growth of columnar crystallites of t-ZrO_2 (?) and their breakdown can show up as repeated cycles in the oxidation kinetics and as "layers" in the resulting oxide, Figure 2-4 and, Figure 2-5, Bryner, 1979 and Motta et al., 2005.

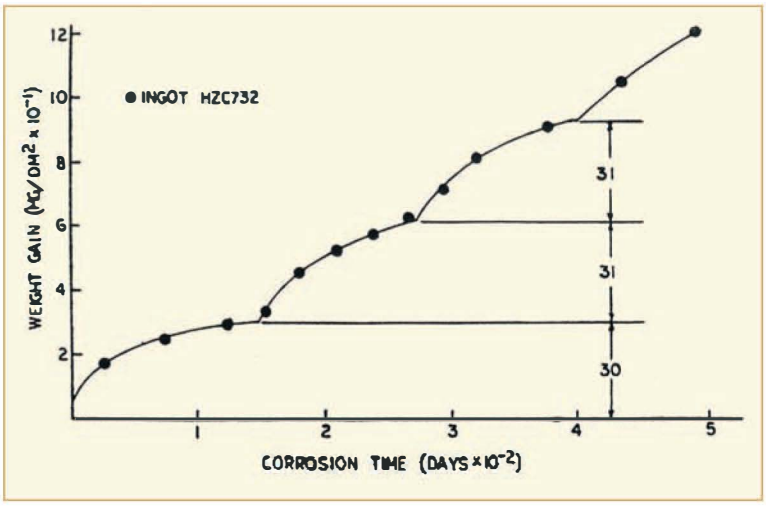

Figure 2-4: Short-time corrosion weight gain of Zircaloy-4 in water at 633K.

3 Key parameters that affect corrosion mechanisms and rate

3.1 Material parameters that affect corrosion mechanisms and rate (Friedrich Garzarolli)

The major material parameters that can affect corrosion are:

- Alloying additions and impurities
- Solute content
- *SPP* characteristics (the influence being their size and composition)
- Degree of cold-work/recrystallisation

The effect of all these parameters on corrosion rate differs in different environments, such as hydrogenated, oxygenated, and LiOH-containing coolants. The effect also varies with temperature and system pressure.

As pointed out in Section 2, and shown in Figure 3-1 the initial corrosion rate follows a parabolic[4] law in hydrogenated water. In pure zirconium a corrosion breakaway occurs resulting in an unstable oxide growth at some point. In corrosion-resistant zirconium alloys a rate transition occurs at a thickness of about 2 µm, depending on material. In pressurized water and high-pressure steam, repeated cycles with corrosion rate transitions can be seen for highly corrosion-resistant alloys, e.g. with >0.3 % Fe. However, in low-pressure steam the corrosion rate remains constant after the transition and is, on average, similar to that in high-pressure steam at the same temperature. In alloys with very fine *SPP* or with a high-Cr alloy content the corrosion rate accelerates after a certain oxide thickness: at least if tested in hydrogenated environments at high pressures.

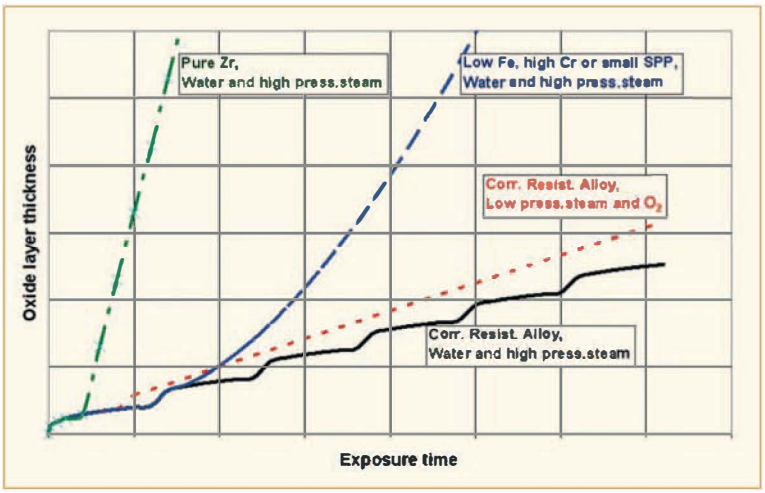

Figure 3-1: Principle corrosion behaviour of different materials in different environments.

In *PWR*s the oxide film is of the uniform type and its growth rate follows out of pile behaviour up to an oxide thickness of about 5 µm, after which it is enhanced by irradiation, Figure 3-2. The irradiation enhancement factor increases primarily with increasing Sn content. At very high fluences the corrosion rate often increases further probably due to irradiation-induced dissolution of intermetallic particles within the metal matrix and other phenomena.

[4] However, the corrosion rate follows a cubic law in the pre-transition region.

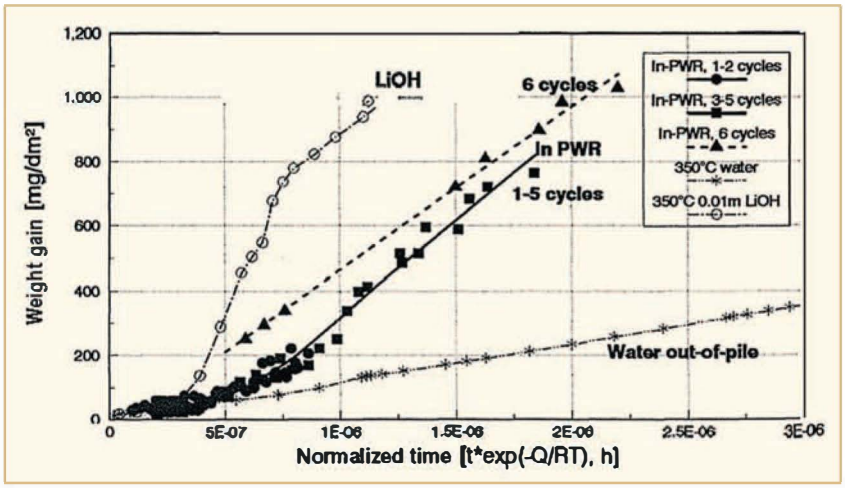

a.) Corrosion of Zircaloy-4 in *PWR* in deionised water and in LiOH.

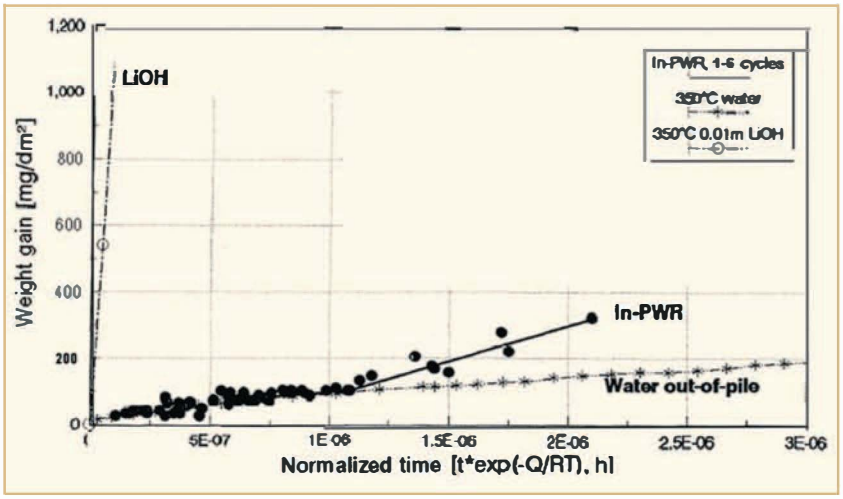

b.) Corrosion of Zr-2.5Nb in *PWR* in deionised water and in LiOH.

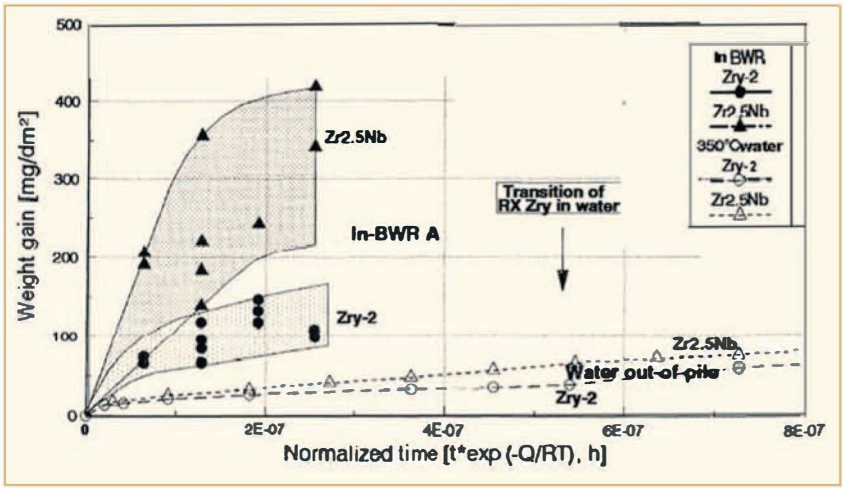

c.) Corrosion of Zircaloy-2 and Zr-2.5Nb in *BWR* and out of pile in water.

Figure 3-2: Effect of irradiation under hydrogenated conditions (*PWR*) and oxygenated conditions (*BWR*) on corrosion of Zircaloy-2/4 and Zr2.5Nb, Garzarolli et al., 1991.

In *BWR*s, corrosion rate is increased particularly in the early exposure period and saturates at high exposure times. Zr-2.5Nb is, in *PWR*s, much more corrosion resistant than Zircaloy-4. However, in *BWR*s, much higher oxidation than Zircaloy-2/4 is observed.

In *BWR*s, besides uniform corrosion, shadow corrosion, starting at <10 days, can appear at positions close to Inconel or *SS* components and nodular corrosion, starting after an exposure of 10 to 100 days. Furthermore, a late increased uniform corrosion is observed (at least with Zircaloy-2) at high burn-ups and long exposure times. Figure 3-3 shows the time dependency of the different types of in *BWR* corrosion.

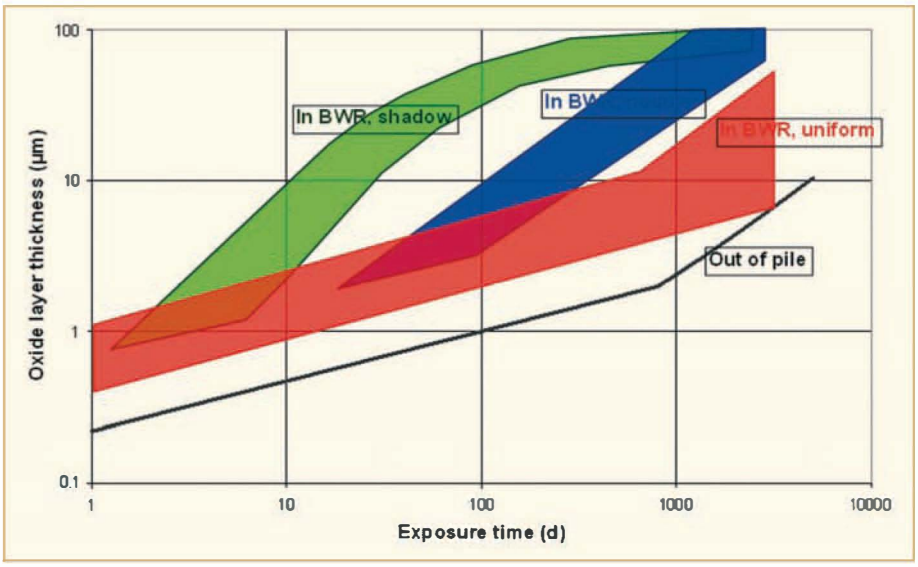

Figure 3-3: Time dependency of the different types of corrosion in *BWR*.

The pressure tubes of *CANDU* reactors show an early corrosion enhancement for Zircaloy-2 and Zr-2.5Nb, somewhat similar to *BWR*s, but no differences between Zircaloy-2 and Zr-2.5Nb. However, in *CANDU* reactors a late acceleration of corrosion at long exposure times (>2000 days) is observed in Zircaloy-2 but not Zr-2.5Nb.

Some fraction of the corrosion hydrogen Hydrogen PickUp Fraction (*HPUF*) is picked up by the metal. The *HPUF* is usually lower in oxygenated than in hydrogenated environments. In *BWR* at very long exposure times the pick-up of corrosion hydrogen increases to very high levels (from 5-20% to almost 100%) somewhat before the late increased oxide buildup rate starts. It is interesting to note that that, also in *CANDU* reactors, a significantly late increase of the hydrogen pick-up is observed (at >2000 days) for Zircaloy-2 but not for Zr-2.5Nb, Urbanic et al., 1987.

4 Description of different forms of corrosion (Friedrich Garzarolli)

During corrosion of zirconium alloys in water and steam three different types of corrosion features can be seen in principle, namely:

- Uniform corrosion (in all types of *LWR*s), see Figure 4-1A
- Nodular Corrosion (almost only in *BWR/RBMK*), see Figure 4-1B
- Shadow Corrosion (almost only in *BWR/RBMK*) that can appear as nodular or as increased uniform corrosion, see Figure 4-1C

Uniform corrosion is the normal mode of zirconium alloy corrosion. Nodular corrosion is characterized by much thicker, local oxide patches appearing as white spots. Shadow corrosion is an increased zirconium oxide thickness (either nodular type or a thick uniform oxide) at positions where *SS* or Ni-base components are close to the zirconium alloy material, appearing as a shadow of these components.

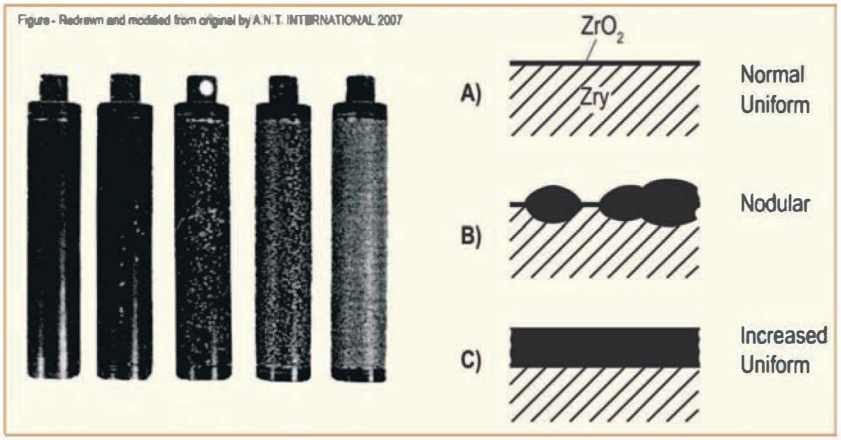

Figure 4-1: Types of oxide films formed in pressurized water and steam on zirconium alloys.

The burn-up (or time) dependency of the corrosion rate varies for different types of corrosion. The time dependency of uniform corrosion usually has at least two different regimes both out of pile and in pile. Initially, corrosion follows an approximately cubic law and later after a rate transition a more or less linear law. During the initial period of oxidation/corrosion of zirconium alloys, a thin, protective, black oxide is formed. As the zirconium oxide grows in thickness, the outer part of the oxide (that which faces the water/steam phase) is transformed into a greyish, porous oxide. The transformation to porous oxide starts at isolated, localised regions and then extends over the surface as can be observed from the development and growth of grey spots e.g. Figure 4-2. These grey regions can be seen under in-*PWR* corrosion conditions to form at an oxide thickness of about 5 µm, representing the thickness at which the regime where irradiation enhanced corrosion begins. This critical thickness is reduced to about 1 µm in out-of-pile tests at high concentration of LiOH. No such grey dots are seen in pressurised water or steam out of pile, probably because the color change at the transition is very moderate. The dense to porous oxide transformation occurs at a certain oxide thickness and is usually cyclic (and is not enhanced), at least if corrosion proceeds in high-pressure water and steam. *SEM* examinations have shown that the oxide has a layered structure e.g. Figure 4-3 with bands of fine pores separated by dense layers with a thickness that is often reported to decrease with increasing corrosion rate.

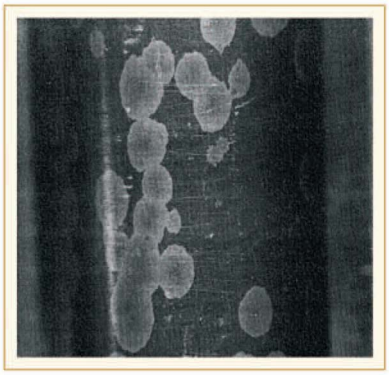

Figure 4-2: Appearance of corroded Zircaloy tube exposed to high-pressure water containing 70 ppm LiOH at 350°C for 140 days, Beie et al., 1994.

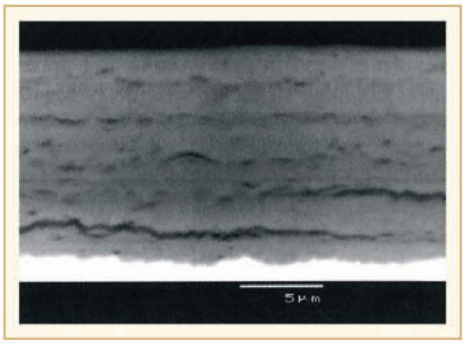

Figure 4-3: *SEM* micrograph on cross section of the M5 oxide layer formed in a *PWR* after 6 cycles at span 4 in back-scattered electron mode, Bossis et al., 2006.

At low temperatures, e.g in a *BWR*, corrosion may remain in the pre-transition regime for long time periods. Nodular corrosion and shadow corrosion start in-*BWR* after a few to 100 days after start of operation and usually saturate at higher exposure times. Figure 4-4 shows the appearance of nodular corrosion and a typical metallographic cross-section. It should be mentioned that the shape of nodular corrosion can vary. The growth rate of nodules decreases at high burn-ups, at least for Zircaloy-2.

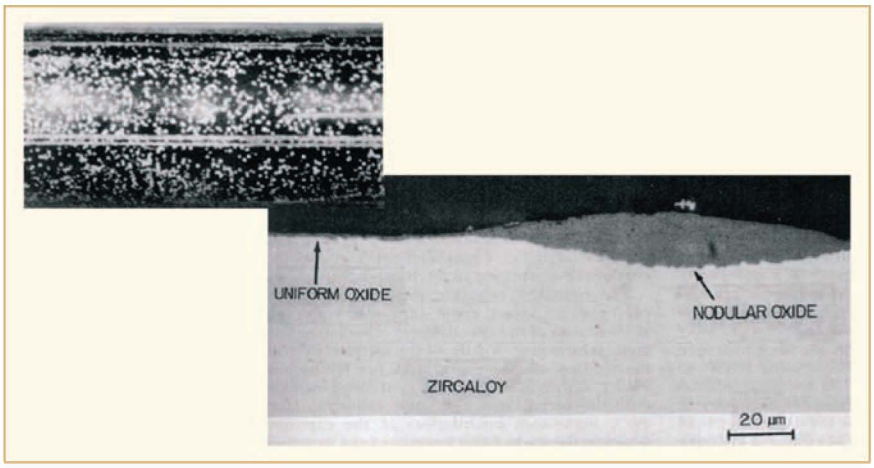

Figure 4-4: Typical appearance of nodular corrosion in visual inspection and metallographic examination.

Figure 4-5 shows a typical example of shadow corrosion on a *BWR* fuel channel due to the proximity of a *SS* control rod handle. The oxide thickness in the area of the shadow appears mostly as a much thicker, uniform oxide but sometimes as a nodular oxide (see Figure 4-4).

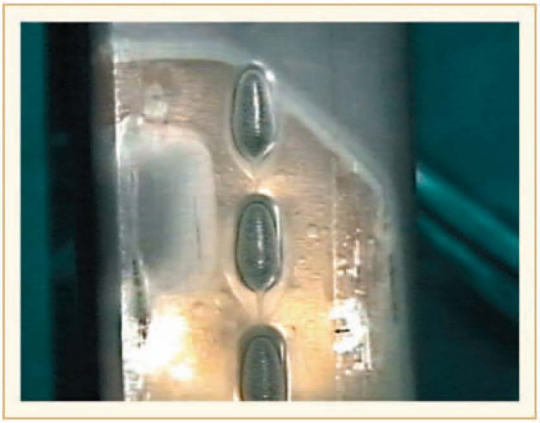

Figure 4-5: Shadow corrosion

Both in *BWR*s and *PWR*s/*VVER*s, late-in-life corrosion acceleration may occur due to the impact of zirconium hydride rim formation, *SPP* dissolution and other effects causing a degradation of the zirconium oxide barrier layer (see Figure 1-3).

Uniform corrosion exhibits a strong temperature dependence, Figure 4-6. However, the nodular corrosion rate temperature dependence is on the contrary very small. Thus, extreme corrosion rates that may lead to failures are always due to uniform corrosion.

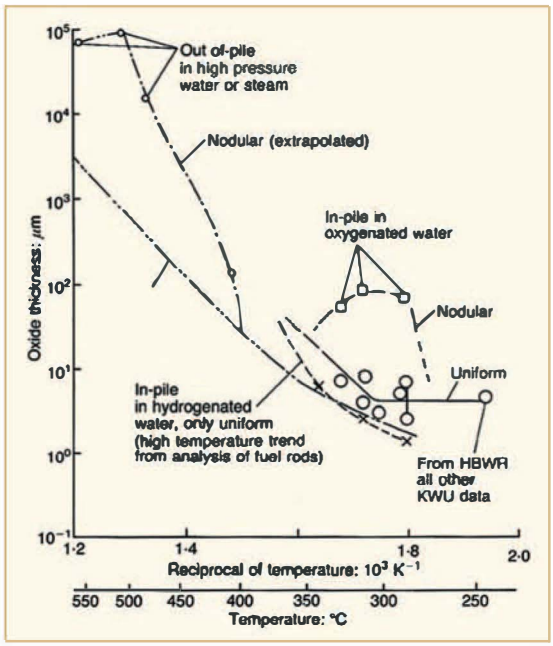

Figure 4-6: Hypothetical Zircaloy corrosion map for an exposure of 500 days in reactor under oxygenated and hydrogenated water conditions, and outside the reactor in high pressure water and steam, Garzarolli et al., 1979.

5 Open items (Friedrich Garzarolli)

The corrosion mechanism of zirconium alloys depends on the environmental conditions and is governed by several very complex and often related processes and features. In this report we have dealt with many questions but more understanding is yet to be evolved.

To clarify the mechanisms there is a need for co-operation between scientists from several different technological areas. A better understaning of the corrosion mechanisms will help:

- Zirconium alloy development for *PWR* and *PWR*
- Development of water chemistry specification
- Root cause analysis of accelerated corrosion phenomena.

In Figure 5-1 the boundary conditions, rate-governing mechanisms, as well as the processes and features affecting corrosion are summarised. The corrosion rate depends on the oxygen ion diffusion rate and on the barrier thickness. Temperature effects on corrosion rate are mostly governed via oxygen ion diffusion (although there is also some effect from the barrier layer thickness as pointed out by Beie et al., 1994). However, the environment, zirconium alloy chemistry and microstructure affect both barrier layer degradation and oxygen ion diffusion. Oxygen ion diffusion may by governed, under certain conditions, by electronic conductivity. More or less always, oxygen ion diffusion through the outer part of the barrier layer occurs along oxide grain boundaries. Close to the metal/oxide interface, where the oxygen potential is very low and the oxygen vacancy concentration is very high, a rather fast bulk diffusion occurs. This bulk diffusion is affecting very important processes for the barrier layer degradation such as:

- mode of crystallisation of the oxide layer,
- fraction of tetragonal oxide
- stresses created by the larger volume of the oxide than the metal,
- oxide crystal alignment.

The authors of the report think that more effort should be put into the study of the following aspects:

- Improved characterisation and understanding of the structure of the barrier layer at the metal/oxide interface
- Quantification of the thicknesses of the grain boundary and bulk anion diffusion zones within the barrier layer and how are they affected by the material and environment?
- Development of an understanding of how anion diffusion in the innermost part of the oxide layer affect the metal/oxide interface, the barrier layer thickness, the character of sub-oxides, the metal/oxide interfacial roughness and finally the crystallisation process within the barrier layer?

More and more reports conclude that the type and width of a barrier layer is important for corrosion resistance. It is not clear how the barrier layer affects corrosion rate. The major questions are:

- Motta et al., 2007, believe that crystallite alignment of barrier-layer tetragonal oxide is an important influence on corrosion because optimally-aligned crystals minimise compressive stresses in the oxide. Can this very interesting idea be confirmed by stress measurements and can it be explained how *SPP* and Nb affect this process?
- Is the tetragonal oxide at the barrier layer stabilised by high compressive stresses, as some scientists believe, or by a fine grain size?

- Often a high fraction of tetragonal oxide is observed in samples with low corrosion resistance. Is this high fraction of tetragonal oxide the consequence or the cause of a high corrosion rate?
- Under which conditions can amorphous oxide form at the metal/oxide interface? This can probably only be examined in samples cooled very quickly from the corrosion temperature (e.g. by removing the autoclave from the furnace during cool-down).

It is very questionable as to which process initiates the corrosion rate transition. In particular the following questions arise:

- Does the tetragonal to monoclinic oxide transformation occur preferentially at the corrosion rate transition as is often stated or is the transformation a more a continuous process?
- What is the hydrogen/proton concentration at the oxide/metal interface, which parameters affect it, and, if it is an important parameter, which concentration causes break-down of the columnar grains and nucleation of new equiaxed grains at the metal/oxide interface?

Relatively good-quality information exists, from in-situ electrochemical experiments (impedance measurements and polarization tests), on corrosion potential, electrical conductivity and oxide characteristics under out-of pile, hydrogenated-water conditions. However, similar tests under more real conditions are needed, such as:

- In-situ electrochemical tests under *BWR* and *PWR* conditions with samples exhibiting both high and low corrosion resistance, nodular corrosion and with different deposited crud types. Such measurements should also be able to give reliable answers to questions regarding the effect of irradiation on corrosion including why its effect differs with environment and zirconium alloy.
- In-situ electrochemical tests on different alloys in different water chemistries to assess the impact of water chemistry on corrosion mechanisms.

As far as the action of *SPP*s on corrosion and hydrogen pick-up is concerned, the oxidation and dissolution characteristics of *SPP*s in the oxide layer grown in different environments on different zirconium alloys is probably an important process step. A good database exists, e.g. from *TEM* of oxide layers, regarding the oxidation and dissolution characteristics of Laves-phase *SPP* in the oxide layer.

- However, almost nothing is known on the behaviour of the Zintel-phase *SPP*.

Furthermore, it is suggested that more detailed studies are required to answer the following questions:

- Why is corrosion linear in 1 bar steam (does migration of H_2O through fine pores control corrosion in low-pressure steam?)
- Why, in contrast, is corrosion cyclic in high-pressure water and steam (is it probably because corrosion is controlled by anion diffusion through a barrier)?
- Is there any difference in the long-term corrosion behaviour between Zircaloy-2 or Zircaloy-4 with optimum *SPP* size and with fine *SPP* size?

For nodular corrosion, several widely-varying mechanistic models have been proposed. Nodular corrosion starts at a critical oxide thickness and grows with a widely-varying rate usually exhibiting a more or less pronounced saturation. Obviously, nodular corrosion starts earlier in Zircaloy-2 than in Zircaloy-4 but exhibits a more pronounced saturation in Zircaloy-2. To understand what are the important parameters which influence nodular corrosion, the following questions need to be answered:

- What are the important mechanistic processes?
- Should we differentiate between initiation and later growth?
- Why do Zircaloy-2 and Zircaloy-4 behave differently? Does the relatively large Zintel phase *SPP* in Zircaloy-2 enhance nodule nucleation and promote saturation of nodule growth?
- In aggressive environments, why does nodular corrosion start earlier and why is nodular corrosion rate higher? Does a high concentration of monovalent species, such as Na+, Li+, F-, etc., in positions with slightly increased porosity initiate and/or accelerate nodule growth?

The rod power history influences corrosion rate not only in *PWR*s but also in *BWR*s. Why is there a power history dependence in *BWR*s keeping in mind that the impact of temperature on corrosion rate is low and not as strong as it is in *PWR*s? It is well known that gadolinia rods in *BWR*s were more prone to nodular corrosion and *CILC* failures (compared to UO_2 rods) in earlier years. It is also well known that gadolinia rods have a very different power history compared to that of UO_2 rods.

Why do corner rods in *BWR* assemblies often show much higher oxide thickness and *HPUF* values than rods in other locations?

What is the real mechanism of shadow corrosion?

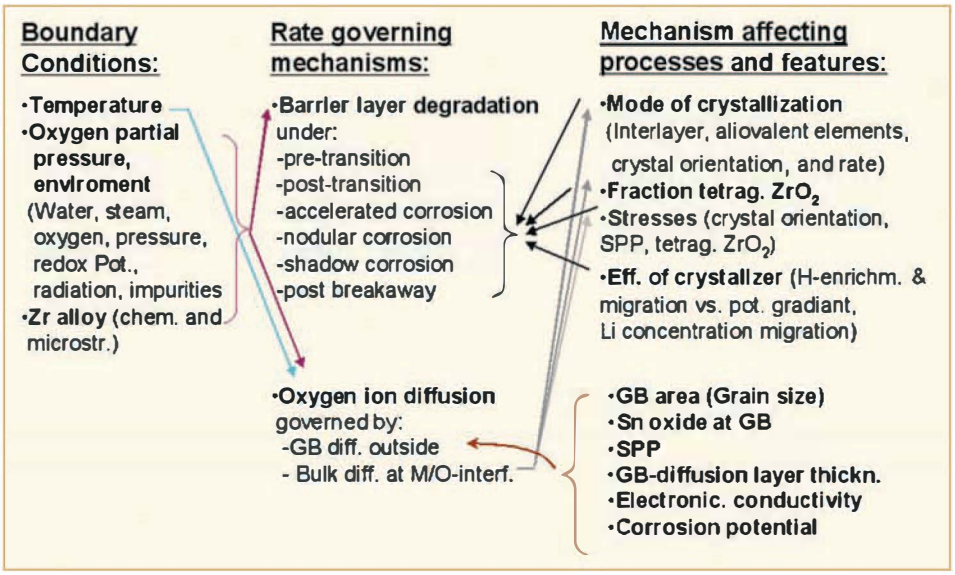

Figure 5-1: Mechanism of zirconium alloy corrosion.

The pick-up of corrosion hydrogen by zirconium alloys depends on the environmental conditions and is governed by several very complex and often related processes and features. Clarification of this situation needs the co-operation of scientists from several different technological areas. It is considered that the major goals for future research should be:

- Zirconium alloy development for *PWR* and *BWR*.
- Development of water chemistry specification.
- Root cause analysis for accelerated hydriding phenomena.

6 Discussions, implications and summary (Ron Adamson)

Various aspects of corrosion and the mechanisms of corrosion have been discussed in the preceding sections. A brief summary of this report is given here:

6.1 Introduction (Section 1)

The emphasis of this *STR* is on the ***mechanisms*** of corrosion of zirconium alloys used in the core of nuclear power plants. The entire area of corrosion (and the accompanying absorption of hydrogen in the zirconium metal matrix) is of prime interest when considering performance of core components and, therefore, the performance of the entire reactor.

Corrosion of zirconium alloys is an electrochemically-driven process affected by the microstructure and microchemistry of the alloy surface, the nature of the oxide layer that forms, the temperature at the metal/oxide interface, the chemistry and thermohydraulics of the corrodent water, the effects of irradiation and the effects of time. Specifics of these processes are given in various sections of this STP.

In comparing *BWR*s with *PWR*s, with corrosion mechanisms in mind, the main features are:

- *BWR* coolant boils; *PWR* coolant does not. This has an important effect at the oxide/water interface.
- *PWR* coolant contains a high concentration of hydrogen; *BWR* coolant does not. Complementarily, *BWR* coolant contains a high concentration of oxygen, *PWR* coolant does not. This has an important effect on corrosion processes.
- *PWR* components generally operate at higher temperatures than *BWR* components. Corrosion processes are temperature dependent.
- Both reactor types employ chemical additions to the coolant which may affect corrosion and build-up of deposits on fuel rods.

It also should be noted that *BWR* zirconium alloys continue to be primarily Zircaloy-2 or slight variants of Zircaloy-2. *PWR* zirconium alloys no longer tend to be Zircaloy-4, for reasons of insufficient corrosion resistance (and hydriding resistance) at high burn-up, but have moved toward zirconium alloys with Nb additions.

The type of oxides which form during corrosion in reactor water can be put into several categories.

1) Uniform
2) Patch or accelerated uniform
3) Nodular
4) Shadow
5) *CRUD*-enhanced

The two most basic are uniform and nodular corrosion. Uniform corrosion has an additional form of corrosion, – "patch" or "accelerated uniform". The fourth category is "shadow corrosion", which can look like thick uniform corrosion but has some characteristics of nodular corrosion. The fifth category is crud-enhanced corrosion, which is a temperature-driven process induced by poor heat transfer in crud-impregnated corrosion layers. These categories are discussed in detail in various sections of this *STR*.

Uniform corrosion occurs in both *PWR*s and *BWR*s. The oxide itself is uniform in thickness and consists of several different layers, discussed in Section 2. The shape of the corrosion versus burn-up (fluence, time) curve in *PWR*s depends on several variables: initial *SPP* size, irradiation, amount of cold work, specific alloy, water chemistry, temperature, local thermohydraulics, hydride concentration – all discussed in Section 3. For Zircaloy-4 the corrosion thickness at high burn-up may reach or exceed 100 μm, while some of the newer alloys have less than half of that. As was noted in Table 1-2, only uniform corrosion occurs in *PWR*s under non-boiling, hydrogenated conditions.

In *BWR*s, uniform corrosion continues at a very low rate out to moderate burn-ups. During reactor exposure, the microstructure of the Zircaloys used in *BWR*s is continually evolving due to irradiation damage and second phase precipitate (*SPP*) dissolution. In the range 30-50 MWd/kgU ($6\text{-}10\times10^{21}$ n/cm^2, E>1 MeV), changes in the microstructure induce an acceleration of uniform corrosion, as described in Section 4.1. First, patches of white oxide appear in the otherwise black or grey uniform background. These patches remain very thin, about the same as the black uniform corrosion film. At some point the patches cover 100% of the surface and oxide thickening occurs at an accelerated rate, labelled "late increased corrosion".

Importantly, at the same or somewhat higher fluences, in *BWR*s a marked increase in hydrogen pick-up fraction occurs. This hydriding is potentially a more serious issue than the corrosion increase.

In *BWR*s (and *RBMK*s) nodular corrosion, characterised by locally-thick oxide appearing as white spots, occurs. Small-*SPP* Zircaloys (average *SPP* size less than about 0.1 μm) in general do not form nodules. In large-*SPP* Zircaloys, nodules initiate early in life and grow at a decreasing rate with fluence. In some cases, for aggressive water chemistries and susceptible material, nodules can coalesce to cover the entire surface. Nodular oxide thickness does not generally cause performance problems; however, in severe cases spalled oxide can be a source of "grit" in control drive mechanisms. Serious fuel failure problems can be induced by a combination of heavy nodular corrosion and copper-zinc-laden crud, resulting in the *CILC* (crud induced localized corrosion) phenomena discussed in Section 4.4.

The fourth type of corrosion is the so-called shadow corrosion, described in more detail in Section 4.2. Shadow corrosion is induced on all zirconium alloys when they are in close proximity to many non-zirconium alloys such as stainless steel or Inconel. The oxide thickness is unusually large and often appears to be particularly dense and un-cracked. A common occurrence in *BWR*s is shadow corrosion oxide induced by a stainless steel control blade handle. Shadow corrosion has "always" been present in *BWR*s, but not in *PWR*s, which is primarily related to the high *PWR* hydrogen concentration, which in turn reduces or eliminates galvanic potentials between dissimilar alloy components. In *BWR*s, shadow corrosion has caused no performance issues until recently when, at one reactor, fuel performance problems were induced by unusually severe "enhanced spacer shadow corrosion". Also, more recently, shadow corrosion has been alleged to be involved in *BWR* channel bow problems. Both issues are addressed in Section 4.

Various sections of this *STR* address in more detail the mechanisms which are believed to be most important in describing corrosion in zirconium alloys.

6.2 Basics of corrosion and hydrogen pick-up (Section 2)

6.2.1 Mechanisms

Corrosion of zirconium alloys at elevated temperatures is basically an electrochemical process involving a galvanic cell. The growth of the oxide film by oxygen vacancy diffusion is the anodic process and reduction of hydrogen ions from the water by electrons diffusing through the oxide film is the cathodic process. Since ZrO_2 is a very good insulator, measurements of the electric potential that develops across the oxide show that electron transport across the oxide film is more difficult than the oxygen vacancy diffusion process. Thus, electron transport through the oxide is rate-determining.

After the oxide grows to about 2 μm by forming columnar oxide crystallites with preferred orientations, break-down of the largely impervious oxide occurs with an attendant acceleration in the corrosion process (post-transition corrosion). This break-down is probably a result of accumulation of impurities (or alloying elements) at the columnar crystallite boundaries combined with a decreasing compressive stress in the oxide that is unable to maintain the stability of the tetragonal (t)-ZrO_2 phase. Other factors, such as ingress of water may also be involved in the tetragonal → monoclinic (m)-ZrO_2 phase transformation that initiates post-transition corrosion.

The electronic conductivities of ZrO_2 films can be degraded by the incorporation of alloying elements or impurities (especially Fe) in the pre-transition oxide film. The oxide electronic conductivity is significantly reduced by irradiation with any species having an energy greater than the ZrO_2 band-gap energy (~5eV). Thus, *UV*, Cerenkov, gamma and beta radiation are all capable of enhancing the corrosion of zirconium alloys under the right experimental conditions. Fast neutron bombardment will only **directly** influence corrosion by enhancement of electronic conduction. However, the electronic conductivity of the oxide film can be **indirectly** enhanced through the fast-neutron-induced displacement of Fe atoms from *SPP*s into the zirconium matrix and into the oxide structure.

Galvanic corrosion processes between zirconium alloys and other metallic components of the system (e.g. spacer grids, fuel channels, *SPP*s) are possible in *BWR*s because of the effects of irradiation on electron conduction for all the components of the reactor. This is because the system is not reducing enough to prevent galvanic potentials being present between the zirconium alloy and these other metals. These effects give rise to shadow corrosion and nodular corrosion effects. Such effects are not seen in *PWR*s provided the dissolved hydrogen content of the reactor water is high enough to make all the various metallic species in the system are at the same, reversible hydrogen potential, such that no galvanic couples can develop between dissimilar metals and alloys.

The uptake of hydrogen by the zirconium alloy matrxi during its corrosion, arising from the reduction of protons by the electrons from the Zr cathodic-half-cell reaction is now considered to be a function of the number of through-wall flaws present in the ZrO_2 film. Diffusion of H in the ZrO_2 lattice, or through *SPP* particles, can be dismissed on present evidence.

6.2.2 Testing

The various techniques used for measuring out-of-reactor corrosion of zirconium alloys (e.g. autoclaves and out-of-reactor loops) are discussed. Also discussed are the sources of variability in experimental data, such as specimen shape; environmental impurities such as F^-, and impurities/alloying content of the alloys tested. Examples of each of these effects are given and the variation that these can induce in the oxidation kinetics that are subsequently measured.

7 References

Adamson R. B., Lutz D. R., Davies J. H., "*Hot Cell Observations of Shadow Corrosion Phenomena*", Proceedings Fachtagung der KTG-Fachgruppe, Brennelemente und Kernbautelle, 29 Februar/1 Marz 2000, Forschungszentrum Karlsruhe, 2000.

Adamson R. B., Cox B., Garzarolli F., Strasser A., Rudling P. and Wikmark G., "*Corrosion of Zirconium Alloys*", *ZIRAT-7* Special Topical Report, Dec., 2002.

Adamson R., Cox B., Garzarolli F., Massih A., Riess R., Strasser A. and Rudling P., "*ZIRAT-10 Annual Report*", 2005.

Adamson R and Cox B., "*ZIRAT-10 Special Topic on Impact of Irradiation on Material Performance*", 2005.

Adamson R., Cox B., Garzarolli F., Riess R., Sabol G. Strasser A. and Rudling P., *Zirat11* Annual Report, 2006

Anada H. and Tekada K., "*Microstructure of oxides on Zircaloy-4, 1.0Nb Zry-4, and Zircaloy-2 formed in 10.3-MPa steam at 673*°C", *ASTM* STP 1295, pp. 34-54, 1996.

Anada H. et al., "*Effect of annealing temperature on corrosion behaviour and* ZrO_2 *microstructure of Zry-4 cladding tube*", *ASTM* STP 1295, pp. 74-93, 1996.

Anada H. et al., "*Chemical state analysis of Sn and Fe in* ZrO_2 *by Mössbauer spectroscopy*", *ASTM* STP 1423, pp. 154-168, 2002.

Andersson B., "*The Enhanced Spacer Shadow Corrosion Phenomenon*", Fachtagung der KTG-Fachgruppe "Brennelemente und Kernbauteile", 29 February/1 March 2000, Forschungszentrum Karlsruhe, 2000.

Andersson B., Limback M., Wikmark G., Hauso E., Johnsen T., Ballinger R. G. and Nystrand A-C., "*Test Reactor Studies of the Shadow Corrosion Phenomenon*", Zirconium in the Nuclear Industry: 13th Int'l Symposium, *ASTM* STP 1423, Moan G. D. and Rudling P., Eds., *ASTM*, 2002.

Arashi H. and Ishigame J.M., Phys Status Solidi Vol. A71, p. 313, 1982.

Asher R. C. and Trowse F. W., "*The Distribution of Hydrogen in Zirconium Alloy Fuel Cladding: The Effects of Heat Flux*", J. Nucl. Mat. 35, p.115-121, 1970.

Baur K, et al., "*Electrochemical examinations in 350*°C *water with respect to the mechanism of corrosion-hydrogen pickup*", *ASTM* STP 1354, pp. 836-852, 2000.

Beie H.J. et al., "*Examination of the corrosion mechanism of Zr alloys*", *ASTM* STP 1245, pp. 615-643, 1994.

Bentini G.G. et al., "*The thermal oxidation of Ion-implanted Zirconium*", Corrosion Science Vol. 20, pp. 17-39, 1980.

Billot Ph. et al., Proc. 4. BNES-Conference on Water Chemistry for Nuclear Reactor Systems, pp. 97, 1986.

Blank H., "*On the Origin of Different Rates of Inpile Post-transition Oxidation for Zr-based Cladding Alloys*", Z. Metallkunde 85, pp. 645-657, 1994.

Blat M. and Noel D., "*Detrimental role of hydrogen on the corrosion rate of Zr alloys*", *ASTM* STP 1295, pp. 319-337, 1996.

Blat M., Legras L., Noel D. and Amanrich H., "*Contribution to a Better Understanding of the Detrimental Role of Hydrogen on the Corrosion Rate of Zry-4 Cladding Materials*", Zirconium in the Nuclear Industry: 12th Int'l Symposium, *ASTM* STP 1354, G. Sabol and G. Moan, Eds. *ASTM*, West Conshohocken, PA, 563-591, 2000.

Briton C.F. and Wanklin J.N., "*Inhibition by boric acid of the oxidation of Zr in high pressure steam*", J.Nucl. Mat. No.3, pp. 326-337, 1962.

Bossis P. Lelievre G., Barberis P., Iltis X. and LeFebvre F., "*Multi-Scale Characterisation of the Metal-Oxide Interface of Zirconium Alloys*", Proc. 12th Int. Symp. on Zr in the Nucl. Ind., *ASTM*-STP-1354, pp. 918-940, 2000.

Bossis P. et al., "*Study of the Mechanism controlling the oxide growth under irradiation*", *ASTM* STP 1423, 2002, pp.190-221

Bossis P. et al., "*Comparison of the high burnup corrosion of M5 and Low-Tin-Zry-4*"; *ASTM* STP 1467, pp. 494-524, 2006.

Bossis P., Verhaeghe B. Doriot S. Gilbon D., Chabretou V., Dalmais A., Mardon J.P., Blad M. and Miquet A., "*In PWR comprehensive study of high burn-up corrosion and growth behaviour of M5® and recrystallized low-tin Zircaloy-4*", Zr in the Nuclear Industry: 15th International Symposium, Sunriver OR, June25-28, 2007.

Bouineau V., et al. "*In situ measurements of the metal-oxide strain tensor in case of zirconium alloy oxidation*", Poster at 15. *ASTM* Zr Conference, Sanriver, Oregon, 2007.

Bradhurst D. H., Draley J. E. and Van Drunen C. J., *"An Electrochemical Mode for the Oxidation of zirconium"*, J. Electrochem. Soc., 112, 1171-1177, 1965.

Broy Y., Garzarolli F., Seibold A. and Van Swam L. F., "*Influence of Transition Elements Fe, Cr, and V on Long-Time Corrosion in PWRs*", Zirconium in the Nuclear Industry: 12th Int'l Symposium, *ASTM* STP 1354, G. P. Sabol and G. D. Moan, Eds., *ASTM*, West Conshohocken, PA, 609-622, 2000.

Bryner J. A., J., "*The Cyclic Nature of Corrosion of Zircaloy-4 in 633K Water*", Nuclear Mater., 82, 84-101, 1979.

Châtelain A., Anderson B., Ballinger R. G., and Wikmark G., "*Enhanced Corrosion of Zirconium Base Alloys in Proximity to Other Metals: the Shadow Effect*", p.485-498, Int. Topical Meeting on *LWR* Fuel Performance, Park City, UT, April, 2000.

Chen J. S. F. and Adamson R. B., "*Observations of Shadow Phenomena on Zirconium Alloys*", Proceedings of the International Topical Meeting on *LWR* Fuel Performance, ANS, West Palm Beach, Florida, 309-317, 1994.

Cheng B. and Adamson R. B., "*Mechanistic Studies of Zircaloy Nodular Corrosion*", Zirconium in the Nuclear Industry: 7th Int'l Symposium, *ASTM* STP 393, Adamson R. B. and Van Swam L. F. P., Eds., *ASTM*, Philadelphia, 387-416, 1987.

Cheng B., Levin H. A., Adamson R. B., Marlowe M. O. and Monroe, V. L., "*Development of a Sensitive and Reproducible Steam Test for Zircaloy Nodular Corrosion*", Zirconium in the Nuclear Industry, 7th Int'l Symposium, *ASTM* STP 939, Adamson R. B. and Van Swam L. F. P., Eds., *ASTM*, Philadelphia, 257-283, 1987.

Cheng B-C., Krüger R. M. and Adamson R. B., "*Corrosion Behaviour of Irradiated Zircaloy*", Proc. 10th Int. Symp. in the Nucl. Ind., *ASTM*-STP-1245, pp. 400-418, 1994.

Christensen H., et al., "*Experimental studies of radiolysis in an in-core loop in the Studsvik R2 reactor*" Proc. BNES conference on Water Chemistry of Nuclear Reactors Systems, pp. 483-485, 1996.

Christensen H. et al., BNES 3rd Workshop on *LWR* coolant water radiolysis and electrochemistry, Dorset, UK, Oct. 2000.

Cox B, "*Degradation of Zirconia Ceramics in 300° C Sulphate Solutions*", UKAEA, AERE Harwell. Report HARD(c), p. 33, 1957.

Cox B., "*Some factors which affect the rate of oxidation and hydrogen absorption of Zircaloy-2 in steam*", J. Electrochem. Soc., v. 109, pp 6-12, 1962.

Cox B., and Johnston T. J., "*The Oxidation and Corrosion of Niobium*", (Columbium), Trans. Met. Soc, *AIME*, v. 227, pp. 36-46, 1963.

Cox B. and Roy C., "*The Use of Tritium as a Tracer in Studies of Hydrogen Uptake by Zirconium Alloys*", Atomic Energy of Canada", Report AECL 2519, 1965.

Cox B. and Roy C., "*Transport of oxygen in oxide films on zirconium determined by the nuclear reaction* ^{17}O (^{3}He, α) ^{16}O", Electrochem. Tech., 4, 121-127, 1966.

Cox B. and Pemsler J. P., "*Diffusion of oxygen in growing zirconia films*", Nuclear Mater., 28, 73-78, 1968.

Cox B. and Donner A., "*The Morphology of Thick Oxide Films on Zircaloy-2*", J. Nuclear Mater., 47, 72-80, 1973.

Cox B., "*Oxidation of Zirconium and It's Alloys*", Advances in Corrosion Science and Technology, Vol. 5, Edited by Mars G. Fontana and Roger W. Staehle, Plenum, N. Y. pp. 173-391, 1976.

Cox B., "*Assessment of in-reactor corrosion models and data for Zircaloys in water*", Proc. 2nd Int. Symp.on Environmental Degradation of Materials in Nuclear Power Systems-Water Reactors, pp. 219-226, Montery, Ca., USA, 1985.

Cox B. and Fidleris V., "*Enhanced Low-Temperature Oxidation of Zirconium Alloys under Irradiation*", Proc. 8th Int. Symp. on Zr in the Nuclear Ind., San Diego, CA, *ASTM* - STP – 1023, 245-265, 1989.

Cox B. and Wu C., "*Dissolution of Zirconium oxide film in 300°C LiOH*", J. Nucl. Mat. 199, pp. 272-284, 1993.

Cox B., Ungurelu M., Wong Y-M., and Wu C., "*Mechanisms of LiOH Degradation and H_3BO_3 Repair of ZrO_2 Films*", Proc. 11th Int. Symp. on Zr in the Nuclear Ind., Garmisch-Partenkirchen, Ger., *ASTM* - STP – 1295, 114-136, 1996.

Cox B., "*Hydrogen Uptake During Oxidation of Zirconium Alloys*", J. Alloys and Comp., Vol. 256, pp 244-246, 1997.

Cox B. and Sheikh H., "*Redistribution of the Alloying Elements During Zircaloy-2 Oxidation*", J. Nucl. Mater. V. 249, pp. 17-32, 1997.

Cox B., "*A mechanism for the hydrogen uptake process in zirconium alloys*", J. Nucl. Mater, Vol. 264, pp. 283-294, 1999.

Cox B. and Wong Y-M., J., "*A Hydrogen Uptake Micro-mechanism for Zr Alloys*", Nuclear Mater., 270, 134-146, 1999.

Cox B., "*Mechanisms of Zirconium Alloy Corrosion in Nuclear Reactors*", Proc. Int. Symp. on Corrosion Science in the 21st, Century, Manchester, UK, July 6-10th, J. Corr. Sci. and Eng., vol. 6, pp. 14, 2003.

Cox B., "*Some thoughts on the mechanism of in-reactor corrosion of zirconium alloys*", J. Nucl. Materials 336, pp. 331-368, 2005.

Davidson S. et al., J. Solid State Chemistry, Vol. 73, p.47, 1988.

Dalgaard S.B., Proc. *IAEA* Conference on "*Corrosion of Reactor Materials*", Vol 2, p. 133, 1962.

Deville S., Chevalier J. and El Attaoui H., "*Atomic Force Microscopy Study and Qualitative Analysis of Martensite Relief in Zirconia*", J. Amer. Ceram. Soc., 88 (5), 1261-1267, 2005.

Edwards W. H., "*Corrosion Investigations in U. K. Nuclear Plants*", Proc. 1st Int. Congress on Metallic Corrosion, London, U. K., May 8-14, 1961.

Elmoselhi M. et al., "*A study of the hydrogen uptake mechanism in zirconium alloys*" Proc. 10th Int. Symp. On Zr in the Nucl. Ind., Baltimore, MD., *ASTM*-STP-1245, pp 62-79, 1994.

Elmoselhi M.B. and Donner A., "*Inhibitors for reducing hydrogen ingress during corrosion of Zr alloys*", *ASTM* STP 1467, pp 563-581, 2005.

Etoh Y., Shimada S., Yasuda T., Adamson R. B., Chen J-S. E., Ishii Y and Takey K., "*Development of new Zr alloys for a BWR*", Proc. 11th Int. Symp. On Zr in the Nucl. Ind., *ASTM* STP 1295, pp 825-849, Garmisch-Parkenkirchen, Germany, 1996.

Fukuya K., Echigoya H., Hattori Y., Kobayashi K., Kobayashi K., and Sasaki T., "*BWR Fuel Channel Performance and Localized Corrosion at High Burnups*", Proceedings of the International Topical Meeting on *LWR* Fuel Performance, ANS, West Palm Beach, Florida, 580-586, 1994.

Garbett K., Henshaw J., Polley M. V. and Sims H. E., "*Oxygen and Hydrogen Behaviour in PWR Primary Circuits*", Proc. JAIF Int'l Conf. Water. Chem. Nucl. Power Plants, Oct. 13-16, 1998, Kashiwasaki City, Japan, 902-909, 1998.

Garde A. M., Patti S. R., Krammen M. A., Smith G. P. and Endter R. K., "*Corrosion Behavior of Zircaloy-4 Cladding with Varying Tin Content in High-Temperature Pressurized Water Reactors*", Zirconium in the Nuclear Industry: 10th Int'l Symposium, *ASTM* STP 1245, A. M. Garde and E. R. Bradley, Eds., *ASTM*, Philadelphia, 760-778, 1994.

Garzarolli F., Manzel R., Reschke S. and Tenckhoff E., "*Review of corrosion and dimensional behavior of Zircaloy under water reactor conditions*", *ASTM* STP 681, pp. 91-106, 1979.

Garzarolli F. et al., "*External corrosion in water cooled power reactors*", *IAEA* Techn. Committee Meeting, Caderach, France, 1985(a).

Garzarolli F., Bodmer R., Stehle H., Trapp-Pritsching S., "*Progress in understanding PWR fuel rod waterside corrosion*", Proc. ANS Topical Mtg. On Light Water Reactor Fuel Performance, Orlando, ANS, La Grange Park, IL, pp. 3-55 to 3-72, 1985(b).

Garzarolli F. et al., "*Influence of various additions to water on Zircaloy corrosion in autoclave tests at 350°C*", Enl. Halden Program Group Meeting, Loen, Norway, 1988.